Fast Acousto-optic Tissue Sensing with Tandem Nanosecond Pulses Experiments and Theory

Steffen G. Resink

FAST ACOUSTO-OPTIC TISSUE SENSING WITH TANDEM NANOSECOND PULSES:

EXPERIMENTS AND THEORY

Steffen Georgius Resink

Thesis committee members:

Prof. dr. ir.	W. Steenbergen	University of Twente
Prof. dr.	A.P. Mosk	University of Twente
Prof. dr.	K.J. Boller	University of Twente
Prof. dr.	E. Bossy	Institut Langevin Paris, France
Prof. dr.	J.F. de Boer	VU Amsterdam
Dr. ir.	H.L. Offerhaus	University of Twente

The work described in this thesis was performed at the Biomedical Photonic Imaging (BMPI) group, MIRA Institute for Biomedical Technology and Technical Medicine, Faculty of Science and Technology, University of Twente, P.O. box 217, 7500 AE, Enschede, The Netherlands.

This work is part of the research programme of the Foundation for Fundamental Research on Matter (FOM), which is part of the Netherlands Organisation for Scientific Research (NWO).

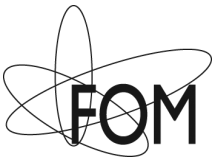

Cover design: Steffen Resink.
Printed by:
ISBN: 978-90-365-3920-3
DOI: 10.3990/1.9789036539203
This thesis can be downloaded from:

FAST ACOUSTO-OPTIC TISSUE SENSING WITH TANDEM NANOSECOND PULSES: EXPERIMENTS AND THEORY

DISSERTATION

to obtain
the degree of doctorate the University of Twente,
under the authority of the Rector Magnificus,
Prof. dr. H. Brinksma,
on account of the decision of the Graduation Committee,
to be publicly defended
on Thursday the 3rd of September 2015 at 14.45

by

Steffen Georgius Resink
Born on 17th of February, 1983
in Enschede, The Netherlands

This thesis has been approved by:

Prof. dr. ir. W. Steenbergen Promotor

Contents

1 Outline of thesis

In biomedical optics we apply optical techniques on biological tissues or samples with tissue-like optical properties. The main applications revolve around diagnosis and therapy. A few examples are optical coherence tomography, photodynamic therapy, diffuse optical tomography and photoacoustic imaging. For diagnostic purposes some form of sensing or imaging is required. From the whole available electromagnetic spectrum the visible and near infrared wavelengths are particularly useful because many molecular transitions are in this regime. Each material has its own absorption, transmission and emission spectrum. Related to this, the refractive index as function of wavelength is also material dependent. Further, many structures in biological tissues have typical dimensions in the order of these wavelengths causing a great sensitivity for size and shape via wavelength dependent scattering. This scattering is also the cause of a low spatial accuracy in deep tissue imaging methods.

Ultrasound typically scatters orders of magnitude less than light in biological tissues but lacks the contrast that optical techniques offer. By combining optical techniques with ultrasound it is possible to use the optical contrast with the spatial accuracy of ultrasound. Photoacoustics (PA) and acousto-optics (AO) are both hybrid techniques that combine light and sound. In photoacoustics [1] light is send into the sample where it locally is absorbed. This causes a thermo-elastic expansion that can be detected as a pressure wave in the form of ultrasound. The used light source is typically a ns pulsed laser although some researchers experiment with modulated CW light[2]. By determining the delay between the laser pulse and the arrival of the generated ultrasound on the detector the distance between the absorbing structure and detector can be determined. By recording the ultrasound at various positions on the tissue surface the location of the light absorbing structures can be triangulated. In this way it is possible to construct photoacoustic images for medical diagnostic purposes. An example from our group is the photoacoustic mammoscope for detection of breast cancer. A tumor is rapidly growing and therefore it needs nutritious blood. For this reason the density of blood vessels around the tumor is expected to be higher. These blood vessels form the absorbing structures for the photoacoustic mammoscope, thus making it possible to detect breast tumors [3, 4].

The local initial pressure p and thus the PA signal caused by the absorption of light depend on the Grueneisen coefficient Γ, the absorption coefficient μ_a and the local fluence ϕ or the probability Pr for light to travel from input into the region of interest (roi),

$$p = \Gamma \mu_a \phi \propto \mu_a \Pr_{in \to roi} \tag{1.1}$$

The absorption coefficient and Grueneisen coefficient are material properties where the former is wavelength dependent. The fluence however depends on the distance from the illuminated area to the absorbing structure, the optical properties of the materials between and around the absorbing structure and setup properties as the size and shape of the illuminated area and the numerical aperture. Thus the fluence is a largely unknown parameter partly determining the signal strength. This makes it hard to compare measurements between tissues or even signals of identical absorbing structures at different locations within the same tissue. An absolute measurement of μ_a is impossible when the fluence is unknown. There are models that give some estimate of the fluence distribution [5, 6] but given the large number of unknowns we choose an experimental method to compensate for the fluence distribution. This method we call Sound Light and combines photo acoustics with acousto-optics. Proof-of-concept experiments of Sound Light have been given in transmission and reflection mode [7, 8].

Because we want to use Sound Light in clinical applications, e.g. an advanced photoacoustic mammoscope, the acousto-optics needs to work in living tissue. If we want to be able to measure many points with high SNR a camera based AO setup would work best. However, the speckle patterns from living tissue decorrelate faster than the integration times necessary to capture them. This leads to a low SNR making practical AO experiments in living tissue very difficult. Further, for Sound Light to work, the optodes of photo acoustic and acousto-optic measurements must be the same. This requires careful alignment between the laser beams for PA, and AO. It would be practical and cost efficient if both PA and AO can be performed by the same laser.

Hence, this thesis is devoted to developing a method for acousto-optic tissue sensing which is faster than the speckle decorrelation in living tissue, and which makes use of a light source that can be used for the photoacoustic measurement as well.

Chapter 2 gives a review of the state of the art of acousto-optics.

Chapter 3 demonstrates the possibility of signal generation with a special pulsed laser that has pulse properties that are typically used in photoacoustic applications is described.

Chapter 4 describes how we overcome the problem of speckle decorrelation by applying the same laser and a delay line leading to tandem pulses with nanoseconds time interval.

In chapter 5 a model describing the amount of 'tagged' light and the phase modulation by ultrasound causing this tagging is given. This is however for ideal speckle patterns with a single polarization and point sampled pixels. This leads to a speckle contrast value of one, which is rarely the case in real life experiments.

Therefore in chapter 6 a correction method is given that accounts for nonideal speckle patterns typically found in experiments.

2 State-of-the art of acousto-optic sensing and imaging of turbid media

Abstract[1]

Acousto-optics (AO) is an emerging hybrid technique for measuring optical contrast in turbid media with the use of coherent light and ultrasound (US). The turbid object of interest is illuminated with a coherent light source and as a consequence a speckle pattern is formed. With the use of US a small volume of interest is selected, which is commonly referred to as the 'tagging' volume. This volume acts as a source of modulated light, where the modulation might involve phase and intensity change. The 'tagging' volume is created by focusing ultrasound for good lateral resolution, the axial resolution is accomplished by making either the US frequency, amplitude or phase time dependent. Typical resolutions are in the order of 1 mm. This review will concentrate on the progress in the field since 2003. Different schemes will be discussed to detect the modulated photons based on speckle detection, heterodyne detection, photo refractive crystal (PRC) assisted detection and spectral hole burning (SHB) as well as Fabry-Perot interferometers. The SHB and Fabry-Perot interferometer techniques are completely insensitive to speckle decorrelation and therefore suitable for *in vivo* imaging. However, the heterodyne and PRC methods also have potential for *in vivo* measurements. Besides measuring

[1] This chapter is based on publication: S.G. Resink, A.C. Boccara and W. Steenbergen," State-of-the art of acousto-optic sensing and imaging of turbid media", J Biomed Opt 17 (2012).

[2] This chapter is published as: S. G. Resink, E. Hondebrink, and W. Steenbergen,

optical properties such as scattering and absorption, AO can be applied in fluorescence and elastography applications.

2.1 Introduction

Noninvasive diagnostic imaging technologies to detect cancer and other diseases come in a wide variety. Most of these technologies like MRI and X-ray lack optical contrast that can be beneficial for detection of small lesions without the use of contrast agents or ionizing radiation [3].

Optical techniques such as optical coherence tomography (OCT) and diffuse optical tomography (DOT) show good contrast but the measuring depth and resolution, respectively, are limited by the strong scattering of tissue. Measuring with high resolution at penetration depths larger than 1 mm is challenging due to the high optical scattering that induces a strong dampening of ballistic photon. These optical techniques are noninvasive and use non-ionizing radiation in contrast to X-ray. The absorption coefficient of light is wavelength dependent making spectroscopy possible, which can be used to determine blood oxygenation levels.

Ultrasound (US) in the few MHz range has a scattering coefficient 2 to 3 orders of magnitude [9] less than light, which comparatively allows for superior penetration depth while retaining spatial resolution. There is however a drawback in which US lacks the benefits of optical contrast.

Two hybrid forms of imaging techniques that use the interplay of sound and light are emerging - acousto-optics (AO) and photoacoustics (PA). These techniques combine the high resolution of US with the strong contrast found in purely optical techniques while remaining non-invasive in nature.

The principle of PA relies on a light pulse irradiating an object of interest. Some parts of the object will absorb this light and will expand thermoelastically. The resulting expansion causes an US wave which is detected by a broadband US probe [10]. The resolution is limited by the light pulse duration, the acoustic tissue properties and the frequency transfer function of the US detection. The higher the detected frequencies the higher the resolution will be. The longer the light pulse duration, the lower the frequencies of the PA signal and the lower the resolution. The acoustic attenuation typically increases with the acoustic frequency, therefore the resolution deteriorates with increasing depth. Typical resolutions are micrometers for PA microscopy with a measuring depth of millimeters [11] and up to millimeters for PA mammography [12] on a measuring depth of centimeters. While the resolution is achieved by the ultrasound, the contrast is provided by optical absorption; the amount of

detected pressure depends on the optical absorption inside the object under investigation.

A second technique that combines ultrasound and light is AO. The possibility of tagging light was investigated by Marks et al. [13], Leutz and Maret [14], Wang et al. [15] and by a patent from Dolfi and Micheron [16]. The sample is illuminated with coherent light, and hence a speckle pattern is formed due to complete randomization of the phases of the electric field of the light escaping from the medium.

To measure only photons that traveled through a volume of interest, ultrasound (US) is employed to encapsulate this bounded region from the characteristic focal zone of the transducer. The photons passing through the US focus will be frequency shifted, or in other words phase modulated, and thus be 'tagged' by the US. A variety of tagging strategies have been developed, along with different detection schemes to find the tagged photons in the sea of untagged photons. The tagged photons detected after exiting the medium provide information on the optical properties present in the vicinity of the volume of interest. When the tagging zone is placed in a tissue volume with high optical absorption compared with the rest of the object, less tagged photons will be detected. This in contrast with when the ultrasound focus is placed in the neighboring tissue. In this review we describe the progress made in AO imaging since the previous review by Wang [1] in 2003: theoretical models, the detection methods to detect the tagged photons, and applications of AO imaging. For further reading, a review by Elson et al. [17] is also focusing on the detection methods, scanning and applications. They give however no equations from the models in the modeling section.

In recent years, considerable improvements in AO have been realized. Some groups developed a method to use AO in a reflection mode setup [8, 18-21]. Others [22, 23] investigated the decay of the modulation of the signal as function of the imaging depth and enhancement of AO with micro bubbles, which can be important in the development of new applications.

2.2 Acousto-optic tagging mechanisms

Light can be modulated in a scattering medium using ultrasound by six different mechanisms. The relative influence of each of these mechanisms depends on the optical properties of the sample and light source and the acoustic properties of sample and transducer.

The first two mechanisms (see figure 2.1) require light to have a sufficient coherence length. The first mechanism relies on the modulation of the optical path length. The scatterers inside the medium are assumed to

oscillate with the US frequency at the US focus due to the pressure wave. The optical path length varies with the distance between the scatterers and therefore the speckle pattern will vary with the applied US frequency. [14] This mechanism is thus equivalent to Doppler scattering and relies on coherent light with a long coherence length to obtain a clear speckle pattern. The mean optical path length is, depending on the optical properties, in the order of 10 to 30 cm for an object with a thickness of 3 cm [24, 25]. The coherence length must be at least in the same order of magnitude. Leutz and Maret [14] have developed a theory which partially modeled this mechanism. The theory is only valid when the mean free path is much greater than the light wavelength and the particle displacement must be much smaller than the light wavelength. Unfortunately the second mechanism is dominant in this case.

The second mechanism is based on refractive index variations due to the acoustic pressure wave. As a result the optical path lengths, and therefore the phases, are modulated. Consequently the intensity of the resulting speckle pattern is also modulated. [1]

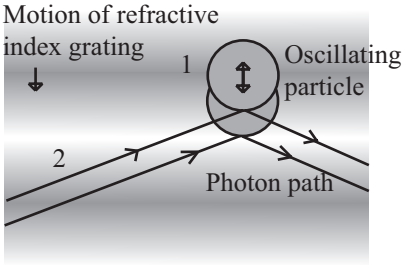

Figure 2.1. Coherent modulation mechanisms: oscillation of scattering particles modulate the photon optical path length (1) and optical path length variation due to refractive index changes (2).

The relative influence of particle vibration and refractive index changes on the induced phase change depends on the optic and acoustic properties of the medium and the used waves. [26-28] Properties such as scattering coefficient and the wavelengths of the ultrasound and probing light change the relative influence of the first and second mechanisms. The strengths of both mechanisms are comparable up to a critical point from where the acoustic wave vector becomes larger than a critical fraction of the mean free path of the photons and the second mechanism becomes dominant.[26]

The other four mechanisms (see figure 2.2) are incoherent phenomena. As a result of US associated local pressure variations the medium is continuously locally compressed and decompressed. Local optical properties such as absorption (mechanism 3), position and scattering cross

section of scattering particles (4 and 5) and the refractive index (6) of the medium will oscillate with the US frequency due to variations in density[1]. The four mechanisms each result in variation of the fluence distribution inside the object. In many situations the associated variation in signal strength is too low to be measured[1]. However Krishnan [29] proposed a theory that fluorescent light is modulated by the gradient of the refractive index by an acoustic lens effect (6). Kobayashi et al. [30] showed the feasibility of detecting this modulated intensity in fluorescence.

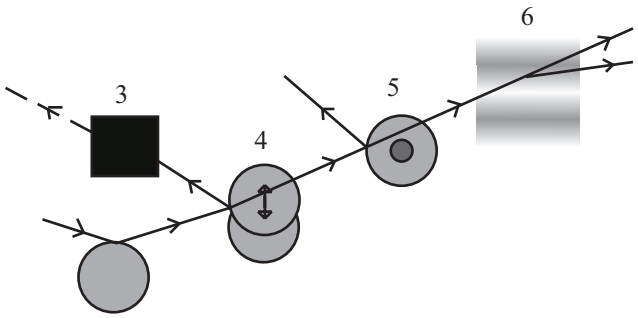

Figure 2.2. Incoherent modulation mechanisms: absorption modulation (3), variation of the position of scattering particles (4), scattering particle cross section variation (5) and variation in refractive index leading to Bragg diffraction patterns (6).

2.3 Theoretical modeling

To understand AO modulation, and to explore the relative importance of the above mechanisms for modulating the light, different theoretical models have been developed. Most models use the more classical approach of phase changes induced by ultrasound, as described by sections 3.2 and 3.3. A different approach used by Mahan et al. [31] is more from a quantum mechanics perspective. Here the fraction of tagged and untagged photons is calculated, see section 3.1.

2.3.1 Fraction of tagged light by Brillouin scattering

Mahan et al. [31] used the mechanism of refractive index changes due to the ultrasound to model the tagged light. The periodic refractive index changes causes Brillouin scattering of the photon stream. A small fraction of these photons will scatter inelastic and are frequency shifted with the US frequency. The intensity of the tagged photon stream is a fraction *r* of the untagged photon stream. They start by deriving an expression for the signal strength of the untagged photons. Step two is calculating the fraction r for different geometries. For a slab with thickness *d* where the ultrasound is uniformly distributed this fraction is given by.

$$r = \frac{3V_{US} g \mu_a \delta\mu_s}{2\pi d} \tag{2.1}$$

where V_{US} is the volume of the ultrasound pulse, g the anisotropy factor, μ_a the absorption coefficient $\delta\mu_s$ the variation in scattering coefficient due to refractive index changes (Tagging mechanism 2 and 5). This fraction of tagged photons is coupled to the signal strength for an AO measurement. The measured signal strength depends on this fraction and the type and quality of the setup. When this signal is compared with the noise, it can be decided whether there is enough signal for imaging purposes.

2.3.2 Theoretical predictions of observable optical quantities during US modulation

The ultrasound modulation of light has been modeled for its consequence for two observable aspects of speckle patterns: temporal fluctuations, and reduction of speckle contrast which are coupled to one another. The modulation of the speckle pattern formed at the detector is often calculated by using the temporal autocorrelation function of the electric field. The intensity of a speckle consists of a large DC component and a smaller component, the one in which we are interested, that varies in time with the US frequency. Leutz et al. [14] and others [1, 26, 27, 32, 33] expressed this autocorrelation function as

$$\begin{aligned} G_1(t) &= \left\langle E(0) E^*(t) \right\rangle \\ &= \int_t^\infty p(s) \left\langle E(t) E^*(t+\tau) \right\rangle ds \end{aligned} \tag{2.2}$$

with *p(s)* the distribution function of paths with length *s* through the sample and E_s the electric field. The < > denote averaging over time. This equation is related to the speckle power spectrum *S* through a Fourier transformation based on the Wiener-Khinchin theorem

$$S(\omega) = \int_{-\infty}^{\infty} G_1(\tau) e^{i\omega\tau} d\tau \tag{2.3}$$

where ω is relative to the optical frequency ω_0 and thus equal to the frequency of the oscillating speckles or beat frequency of the light [1]. Point like scatterers are undergoing a collective motion due to the ultrasound and Brownian motion. The autocorrelation function length can be split in one part describing the exponential decay due to Brownian motion and a second part that describes the autocorrelation as a function of

the periodic ultrasound wave. When both effects are assumed independent from the other then the properties of both factors can be explored separately.

The scatterers in the medium may tend to diffuse due to the Brownian motion. The single particle relaxation time is given by $\tau_0 = 1/Dk_0^2$ where D is the particle diffusion constant and k_0 the wave vector of the light. The autocorrelation of the electric field with a single path length will decay exponentially in time t according to [14]:

$$\left\langle E_s(0)E_s^*(t)\right\rangle_B = \exp\left(-\frac{2ts}{\tau_0 l}\right) \tag{2.4}$$

where l is the mean free path.

This decay time limits the time in which an accurate AO measurement can be performed in most situations. The Brownian motion can be neglected for time scales in the order of the cycle time of the ultrasound [34]. Wang [26, 27] investigated the contribution of phase modulation by refractive index changes and scatterer displacement induced by the ultrasound. He concluded that both effects have a similar contribution up to a critical point. When the mean free paths of the photons between two scattering events become small compared with the acoustic wavelength the second mechanism becomes increasingly more important. This was verified with a Monte Carlo simulation [26].

Sakadžić et al. [32, 35-37] and Wang [26] developed an analytical solution for this autocorrelation function equation 2.2, mostly focusing on the first two mechanisms. For a single pathlength s the contribution to the autocorrelation function is given by [26]:

$$\left\langle E_s(t)E_s^*(t+\tau)\right\rangle = \left\langle \exp\left[-i\Delta\phi(t+\tau)\right]\right\rangle \tag{2.5}$$

Where $\Delta\phi$ denotes the total phase shift of the light due to path length and refractive index variations and is thus a function of μ_s, Δn (mechanism 1 and 2) of the object. After some lengthy algebra [1, 32] and the assumption of weak modulation, the modulation depth, defined as ratio of the intensity at the signal frequency and the unmodulated intensity [1], is found to be proportional to the acoustic amplitude squared [1]. In general the maximum variation of the autocorrelation function will increase with increasing acoustic power and decrease with increasing US frequency while keeping the US power constant. Increasing the optical absorption coefficients will lead to a smaller variation according to [28, 32]:

$$G_1(\tau) = \frac{\sinh\left(L_0\sqrt{\mu_a D^{-1}}\right)}{\sinh\left(Z_0\sqrt{\mu_a D^{-1}}\right)} \frac{\sinh\left(z_0\sqrt{\left(S_u + S_B + \mu_a\right)D^{-1}}\right)}{\sinh\left(L_0\sqrt{\left(S_u + S_B + \mu_a\right)D^{-1}}\right)} \quad (2.6)$$

Where L_0 the distance between the extrapolated slab boundaries, z_0 is the location of the isotropic light source, S_u the term due to ultrasound influence, S_B the term for Brownian motion, μ_a the absorption coefficient and D the diffusion constant.

The intensity and variation of the speckle contrast, which is related to the autocorrelation function, are derived by Zemp et al.[33]. The statistical properties of this speckle pattern are derived from the autocorrelation function. The first order statistics describe the time average intensity and is approximately equal to $G_1(0)$. The second order statistics describe the variation in speckle contrast. The variation is approximately

$$\Delta C \approx \frac{\overline{s}}{4}\left(n_0 k_0 \frac{P_0}{\rho v_a^2}\right)^2 \eta^2 \frac{v_a}{f_a} \quad (2.7)$$

This variation is a function of the average optical pathlength $\overline{s}$, the optical index of refraction n_0, the magnitude of the optical wave vector k_0, the acoustic pressure P_0, the mass density of the medium ρ, the ultrasound velocity v_a, the elasto-optic coefficient η which has a value of approximately 0.32 and the acoustic frequency f_a. This equation is valid under the assumption of weak scattering i.e. $k_a l_{tr} >> 1$ where k_a is the ultrasonic wave vector magnitude and l_{tr} is the transport mean free path. The model predicts a linear relation between the acoustic power and the speckle contrast which is verified experimentally in [33]. All these theories assume homogeneous acoustic waves, except for Sakadžić et al [35-37] in which localized acoustic waves were used.

2.3.3 Monte Carlo simulations

Besides the analytical solutions Monte Carlo (MC) simulations are used to gain more insight into the principles of AO. These models simulate photon distributions inside the medium and include scattering and absorption of the light. One or more of the tagging mechanisms can be implemented, the refractive index and scatterer motion can be modulated. The results of measurements and analytical models are often compared and tested with MC simulation results [38-40]. Wang [26] and others [39] developed and modified MC models for AO applications. Especially the model of Wang et al. is widely used in biomedical optics i.e. [41, 42] and is supported by an analytical model [27, 32, 35, 36].

Leung et al. [43] compared the speed of this model implemented on both central processing unit (CPU) and graphics processing unit (GPU, Nvidia GeForce 9800) with Compute Unified Device Architecture (CUDA). They found an increase in speed, depending on simulation settings and hardware, of a factor 72 for the CUDA implementation.

2.4 Detection of tagged photons

A detection technique must be able to distinguish the tagged or modulated photons from the untagged or unmodulated photons to obtain information from the US focus. Longer integration times will lead to higher signal to noise ratios. However speckle decorrelation alters the speckle pattern and destroys the correlation of this pattern between the start and end of the detection time. Sources of speckle decorrelation are small changes in the optical paths inside the object i.e. Brownian motion of scatterers and blood flow or muscular activity in living tissues. This decorrelation diminishes the detectability of tagged photons. Developed detection techniques can be divided in time- and frequency domain techniques.

2.4.1 Time based methods

Wang et al. [15] measured light modulated at a US frequency of 1 MHz with a photomultiplier. The intensity of a single speckle will oscillate with the US frequency of 1 MHz and this frequency is observed by recording the light flux with the photomultiplier tube. They used 1.1 mm aperture at 5 cm distance from the object and a photomultiplier tube at a distance of 10 cm from this aperture. The advantage of a photomultiplier tube is the speed and sensitivity, so the modulation of a speckle can be detected real time at the US frequency and well within the speckle decorrelation time. The disadvantage is the small detection surface, which in turn reduces the number of tagged photons that can be detected, leading to small signal-to-noise ratio due to the influence of shot noise. In a nutshell: increasing the number n of speckle grains on the same single detector increases the random modulated signal standard deviation (signal of interest) as $n^{1/2}$ and the average power impinging the detector by n. If the detection is shot noise limited (that is rather unlikely to happen) the noise is proportional to $n^{1/2}$ and the signal-to-noise ratio is not increased by increasing the number of speckle grains on the detector. If the noise is linked to the laser fluctuations it is proportional to n and the signal-to-noise ratio will decrease when increasing the number of speckle grains on the detector.

A parallel speckle detection technique was developed by Leveque et al. [44] Instead of a single detector element a CCD camera is used in which the illumination pulses and the ultrasound are timed with a fixed phase

delay. The system was designed to make speckle size comparable to the pixel size. The SNR is improved by averaging the signal from all CCD pixels, making it a larger detector surface. The major disadvantage of a CCD camera as a detector is the reduced frame rate, hence the intensity of a speckle can not be followed in time at the US frequency. However by recording the light intensity for different phases of the ultrasound the modulated intensity and the unmodulated intensity can be estimated. This can be achieved by varying the delay between US and the start of the exposure of the camera. In the case of four-phase measurement the exposure time of the camera is up to one quarter of the US period time.

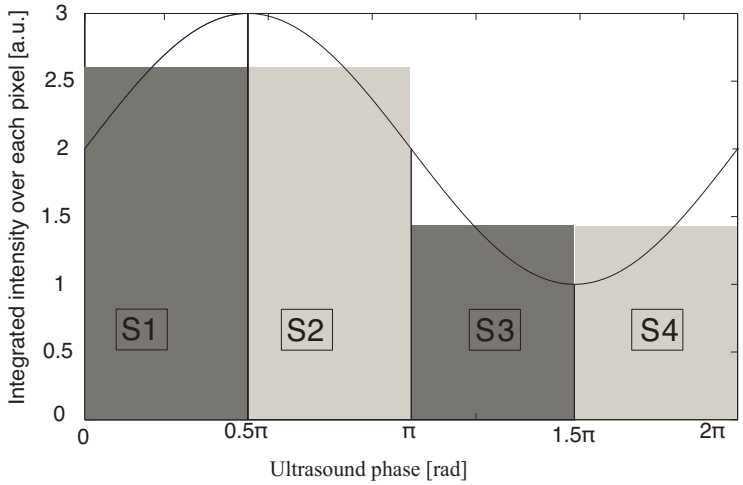

Figure 2.3. Integrated light for each of the four quarters (S1, S2, S3 and S4) of the US period for a single pixel where the curved line denotes the instantaneous light intensity of this pixel. [24, 44, 45].

The signal S_i for each phase from figure 2.3 is given by:

$$\begin{aligned} S_1 &= NT_0\left[\tfrac{I_{dc}}{4} + \tfrac{\sqrt{2}}{2\pi} I_{ac}\cos\left(\phi_1\right)\right] \\ S_2 &= NT_0\left[\tfrac{I_{dc}}{4} + \tfrac{\sqrt{2}}{2\pi} I_{ac}\sin\left(\phi_1\right)\right] \\ S_3 &= NT_0\left[\tfrac{I_{dc}}{4} - \tfrac{\sqrt{2}}{2\pi} I_{ac}\cos\left(\phi_1\right)\right] \\ S_4 &= NT_0\left[\tfrac{I_{dc}}{4} - \tfrac{\sqrt{2}}{2\pi} I_{ac}\sin\left(\phi_1\right)\right] \end{aligned} \qquad (2.8)$$

From these intensities the AC intensity and phase can be calculated using these relations.

$$I_{ac} = \frac{\pi}{NT_0\sqrt{2}}\sqrt{\left(S_1 - S_3\right)^2 + \left(S_2 - S_4\right)^2} \tag{2.9}$$

$$\phi_1 = \arctan\left(\frac{s_2 - s_4}{s_1 - s_3}\right)$$

Where I_{ac} is the modulated part of the intensity for a single pixel, NT_0 the total integration time, and ϕ_1 the phase of the acousto-optic signal. Li et al [46] showed similar relations for two and three phases.

Parallel speckle detection is a very efficient technique for detecting modulated light. However this detection method is sensitive to speckle decorrelation, which lowers the SNR by lowering the signal and increasing the noise. [24] Li et al. [47] showed a laser speckle contrast detection scheme which is less sensitive for speckle decorrelation when short integration times are used. The speckle contrast is defined as the standard deviation of the intensity in the pattern divided by the average intensity of this pattern [48]. Kothapalli et al. [49] tested their Monte Carlo implementation and measured with a speckle contrast setup and investigated the linear relation between speckle contrast and the local scattering coefficient at the US focus and found a good agreement between simulation and experiment.

2.4.2 Interferometric based methods

Instead of following the intensity of the speckles in time domain it is possible to filter out the modulated light with interferometers. The Fabry-Perot interferometer and Mach-Zehnder based techniques are used to detect, or select, only the modulated light at the US frequency. By optically removing non-interesting frequencies the SNR should be increased.

Leutz et al. [14] used a Fabry-Perot interferometer in combination with a photomultiplier tube to detect photons with a frequency shift of 2.17 and 27.3 MHz from a laser source with a wavelength of 514.5 nm. To resolve this relative small frequency difference they used a FP etalon (mirror reflectivity: 99.3%) with a mirror separation distance of 15 cm obtaining a resolution of 12 MHz. The disadvantage of this technique is the great loss of signal photons due to the small *etendue* (the product of the solid angle and area of an aperture) when pinholes are used to select a parallel light beam with a certain frequency. However long-cavity [50] *confocal* Fabry-Perot interferometers are used which have a high *etendue.*

Double-pass confocal [51] Fabry-Perot interferometers are also used to separate the faint spectral line of the tagged photons from the strong untagged spectral line.

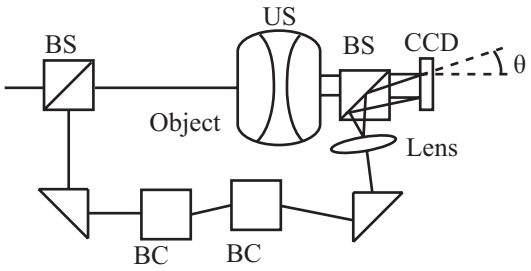

Figure 2.4. Heterodyne parallel speckle detection, the light beam enters at the upper left beam splitter (BS) and illuminates the object. The ultrasound beam (US) is focused inside the object. The reference arm consists of 2 prisms, two Bragg cells (BC) and a lens to expand the beam. Both arms are combined in the second beam splitter and the resulting interference pattern is detected by the CCD array.

The heterodyne parallel speckle detection method adds a reference beam or local oscillator (LO) beam to the standard parallel speckle detection scheme [52-54], making it a Mach-Zehnder interferometer, as depicted in figure 2.4. This technique is shot-noise limited when using a large heterodyne reference intensity. When the signal beam is in phase with the reference beam the intensity on the detector is given by [55]:

$$I = I_s + I_{ref} + 2\sqrt{I_s I_{ref}} \qquad (2.10)$$

Where I is the detected intensity, I_s is the intensity of the signal beam and I_{ref} the intensity of the reference beam; the last term in this equation is the heterodyne gain.

The light in the sample arm is modulated as it propagates through the sample, and the reference arm is modulated with two acousto-optic frequency shifters (Bragg cells) or acousto-optic modulators. The speckle pattern from the sample interferes with the reference beam on the CCD camera which is placed under a small tilt angle θ. The reference light with the modulated part of the sample generates a static speckle pattern which can be detected by the CCD camera. Interference of the non-modulated sample light with the reference light leads to a dynamic speckle pattern, which in the CCD image will be smeared out. The spatial frequency domain (k-space) of the recorded interference pattern reveals the level of the shot noise, the speckle decorrelation noise and the tagged photons in different regions, due to spatial filtering associated with tilt angle θ. The

sensitivity of this technique is limited by the shot noise of the reference light [52, 53] and setup limitations such as dynamic range and sensitivity of the camera. From the four frames of the CCD array, representing the four phases of the reference beam, a four phase complex signal can be calculated. This complex signal in k-space shows interesting properties. The heterodyne signal forms a narrow band of spatial frequencies at a position determined by tilt angle θ (region A in figure 2.5), the decorrelation noise is relatively slow and its fringes consists of the lower spatial frequencies (region B and C). The shot noise is represented by region D.

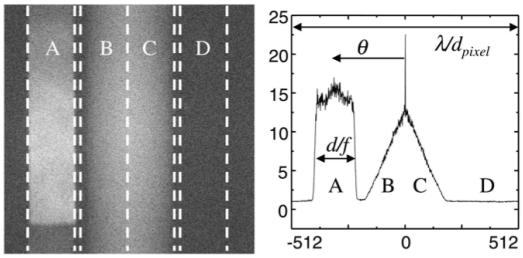

Figure 2.5. k-space image (a) and column average of this image (b) with the regions: Signal(A), decorrelation noise(B,C) and shot noise(D) [52]

For example, the laser light is modulated at 85 MHz up and 80 MHz down with the use of two acousto-optic modulators. For practical reasons two modulators are used instead of one at 5 MHz, that is the difference of both used modulators. The laser light inside the sample is modulated in the focus of a US transducer at 5 MHz.

This is known as single phase detection, four phase detection can be achieved by tuning one of the AO modulators slightly higher, 85.0000075 MHz instead of 85. This way each next frame of the CCD array receives a reference beam with a phase shift of $\pi/2$ radians compared with the current frame assuming a frame rate of 30 frames per second.

The advantage of using multiple phase detection is the higher SNR because the DC component is canceled out. All frames of the one to four phases should be taken within the speckle decorrelation time making one or two phase imaging the better choice where this decorrelation time is short. Atlan et al. [54] give an equation to calculate the complex signal for an arbitrary number of phases.

Another technique uses the same heterodyne setup with the addition of a photo refractive crystal (PRC) in front of the detector. The principle is to

store intensity and phase information of the speckle pattern inside a hologram and readout this hologram with a CCD. The advantage of this self-adapting wave front holography is a larger *etendue* than most CCD's, and possibly a larger SNR. Bloningen [56, 57] investigated the expected AO signal and phase shifts of the photons for photo refractive based detection by utilizing Monte Carlo simulations. They show that the average photon phase shift contains a DC phase shift which is dominant over the usually used AC phase shift. This offers a possibility to compliment the AC data.

The crystal consists of a photorefractive material and thus has a refractive index that depends on the light intensity. The two beams, signal and reference, illuminate the crystal. The two interfering beams construct a 3D intensity profile in the crystal thus writing, using the photo refractive principle, a 3D grating or hologram in the crystal within the response time. Typical response times are 100μs for a $Al_{0.1}Ga_{0.9}As/GaAs$ multiple quantum well crystal (850 nm excitation wavelength) [58], 0.3-100 ms for GaAs (1064 nm) [53, 59-64], less than 10 ms for SPS:Te (790 nm) [65] and 150 ms for $Bi_{12}SiO_{20}$ (532 nm) [57, 66, 67]. Changes in the speckle pattern slower than this response time are not recorded, making the detection insensitive for slow speckle decorrelation. The photo refractive effect selects only optical frequencies from the signal beam which are close to the reference beam frequency.

During readout of the hologram the reference beam is diffracted by the holographic grating. This way the wavefront of the reference beam is shaped in the signal wavefront, but now with a larger intensity. This constructed speckle pattern can be detected by a detector such as a CCD. Chi et al. [68] describes this two wave mixing process in more detail. Gross et al. [59] give a detailed description of detecting tagged light with a PRC.

This self-adapting wavefront holography is a promising technique, but the typical response time is too slow for *in vivo* use where the speckle decorrelation times (<1 ms) are in general much shorter than the crystal response time (~100 ms) [63].

2.4.3 Other methods

Spectral hole burning (SHB) is another crystal based technique developed by Li et al. [63, 69] where the PRC is replaced by a SHB crystal. This technique has also a large *etendue* and is insensitive for speckle decorrelation. The crystal acts as a narrow optic bandpass filter where most optical frequencies are absorbed and only one specific frequency band is transmitted. The reference beam burns a spectral hole in the crystal at the same frequency as the tagged photons. The crystal is an

inhomogeneously broadened optical absorber that can be modeled as a two-level system. The spectral line width is typically sub-MHz when cryogenically cooled and depends on the intensity of the reference beam. During the burning process only the crystal ions inside the crystal that are sensitive for this specific optical frequency are excited from the ground state. This makes the crystal transparent for this optical frequency, the non-tagged photons are absorbed by the crystal.

After burning the spectral hole the reference beam is switched off and the signal beam is switched on and the tagged photons can be detected by a photo detector such as a CCD. The cryogenic cooling (~4 K) is the main disadvantage of this technique.

2.5 Resolution

The lateral resolution of acousto-optic imaging is obtained by focusing the ultrasound and its size is comparable with the width of the US focus when the weight of the unfocused part does not play a major role. The axial resolution is worse than the lateral resolution due to the elongated focus of the ultrasound transducer (Rayleigh length).

The axial resolution can be improved in several ways by changing frequency, amplitude, or phase in time in order to get a resolution equivalent to the pulse-echo in US tomography.

The first method that was implemented is the frequency sweep technique. [70, 71] In this method the ultrasound transducer generates a short chirped signal. The light along the acoustic axis is modulated with a different frequency for each depth. By using the Fourier transform on the detected signal, information in the axial direction is retrieved. Yao et al. [71] combined this chirp technique with a parallel detection scheme. They also showed that this technique does not rely purely on ballistic light by using an obliquely incident laser beam. Wang et al. [70] showed an axial resolution of approximately 1 mm, however this resolution depends on the chirp rate. In chicken-breast tissue they achieved 4 mm resolution [71].

Lesaffre et al. [64] showed a different approach by making the phase of the US and the optical illumination random. Both use the same data set of typical 512 random phases with each of these phases set to either 0 or π. This set of random phases has a typical period time 1 ms. The phase of the optical illumination is modulated with a delay τ relative to the modulation of the US. At a distance of τ times the speed of sound along the acoustic axis, both the optical illumination and US phase are correlated. Therefore only tagged photons from this position are detected using the heterodyne detection scheme with a photo refractive GaAs crystal. The

resolution in the axial direction depends on the speed of sound and the time it takes to change phase, which in this case is (1 ms / 512 ≈ 2 μs) roughly 3 mm. Gross et al. give more theoretical background in [72] regarding this technique. Guillaume et al.[73] showed millimeter resolution in combination with a digital holography scheme.

A third method to increase the axial resolution uses short US pulses [50, 54, 57, 74]. These pulses consist of a few US cycles and thus modulate the light only locally in the axial direction. The US pulse reaches the point of interest after time t=z/c, where z is the distance from the transducer and the point of interest and c the speed of sound (SOS). At this time (t) the sample is illuminated with pulse duration τ and the modulated photons are recorded. The minimally resolvable size in the axial direction depends linearly on the SOS and pulse duration, assuming a short enough light pulse. Achieving high resolution thus requires short US pulses. The smaller the pulse duration the bigger the spread of acoustic energy in the frequency domain. Detection schemes which are only sensitive for a single frequency require a longer US burst and thus a smaller US bandwidth to optimize the SNR [74]. Atlan et al. [54] used an US burst of 3 μs and the axial resolution is 5 mm.

Li et al. [75] investigated the influence of amplitude modulated US on the speckle contrast in a parallel detection setup. In this case the US amplitude was modulated with a 250 Hz to 16 KHz cosine envelope. They show that amplitude modulated US can outperform continuous wave US in signal strength. Weng [76] investigated the relation between US pulse duration and amplitude on the AO signal and concluded that the imaging depth can be increased when reducing pulse duration and increasing the US peak amplitude.

Above methods all describe a way to improve the axial resolution by shaping the acoustic wave. The lateral resolution however is achieved by focusing the US transducer on the volume of interest. A different approach is suggested by Kuchment [77] where an unfocused US transducer is used. An unfocused transducer has spherical wavefronts in the far field. When the US transducer emits a small US wave train a small circular shaped region is tagged. By repeating these measurements for different positions of the US transducer a synthetic focus is constructed on the positions where these circular regions intersect. Another example of what could be seen as synthetic focusing is used by Li et al. [78]. Sakadžić et al. [50] used tomography to achieve very high resolutions in the order of 100 μm.

Let us underline that whatever is the technique that led to reduce the resolution it has to involve signal variation shorter than the decorrelation time. This is obviously realized for short pluses but must also be done for other approaches such as the shirps or the random sequences.

2.6 Applications of acousto-optic imaging

2.6.1 Measuring optical properties

While it is still unknown what the measured quantity is in AO, its signal probably holds information on the local fluence rate. Lev and Sfez [18] showed the possibility of measuring the local fluence rate using AO between two optodes. This local fluence rate depends on position of illumination and detection and the optical properties distribution in the object such as the absorption coefficient. A map of the estimation of the optical absorption is obtained by scanning the US focus through the object and estimate the absorption coefficient for each position from the modulated fluence rate [48]. The AO signal is affected not only by optical absorption and scattering in the US focus but also in the rest of the object. Therefore quantitative estimation of the absorption coefficient requires the number of tagged and untagged photons and an algorithm that solves the inversion problem as in DOT [36, 39, 60, 79-81].

Gunadi and Leung [82] investigated the sensitivity of AO for the application of spectroscopy. From the spatial distribution of AO sensitivity they derived a penetration depth for AO of 14.8 mm for an intralipid solution with a μ_s' of 12 cm^{-1} and absorption of μ_a of 0.0235 cm^{-1}.

The absorption coefficient is in most cases dependent of the wavelength of the used light source making functional imaging possible. For instance chromophores like hemoglobin and oxy-hemoglobin have distinct absorption spectra. This creates the possibility of determining the oxygenation levels of blood in biological tissues.[39]

2.6.2 Acousto optic modulated fluorescence

Fluorescence is often used to label particles and cells, and enables the study of biological processes on the molecular and cellular level. However light scattering makes it hard to determine the origin of the fluorescent light *in vivo*. Efforts similar to DOT have to be made to perform optical tomography with fluorescent light [83]. Kobayashi et al. [30] Hall et al. [84] and Yuan et al. [83, 85-88] investigated techniques to modulate, and thereby localize, this fluorescent light in turbid media.

The fluorescent light is non-coherent and modulation has to come from modulation of optical properties of the sample. The US field causes variation in the density, and consequently induces a gradient of the refractive index based upon the localized pressure variations in the medium. On these gradients the light is deflected, which leads to variations in photon density in the fluorophores (mechanism 6 in figure 2.2),

therefore the intensity of the fluorescence is modulated. Also, the scattering coefficient is modulated (mechanism 5) which causes fluorescence intensity modulation by variation of the photon density distribution [30].

Yuan [83, 85-88] investigated the combination of fluorescence with AO and derived a mathematical model. They proposed two mechanisms which can explain the modulation of fluorescence. The first mechanism for low concentrations is similar to the explanation of Kobayashi et al. [30], the excitation light is modulated and thus also the fluorescent light. For high concentrations they propose a modulation in quenching rate and thus in detected intensity. At high concentrations the variation in distance between fluorophores leads to variations in quenching, giving a modulation of fluorescence which is inverted compared to lower concentrations where quenching is absent. The signal strength found by Yuan [87] shows a linear relation with the applied voltage on the ultrasound transducer, which is usually linear with the US pressure, and the signal was much weaker than found by Kobayashi et al.

Yuan et al. used a photo multiplier tube to detect the modulation of the fluorescence and found that this signal depends quadratic on the acoustic pressure. Hall et al. [84] showed a parallel detection scheme to detect the modulation in fluorescence by modulating the gain of the CCD with the US frequency. The phase difference between the US and CCD gain modulation was 0º and 180º.

2.6.3 Acousto-optic assisted elastography

AO Elastography is an imaging modality for quantifying mechanical properties. Kirkpatrick et al. [89] stimulated tissue with a low frequency acoustic force (1-5 Hz) which induces a strain. The surface of the tissue, in their case the skin, will give a dynamic shift in the speckle pattern in the back reflected laser light with this low frequency. The stiffer the material the less shift in the speckle pattern is observed.

Bossy et al. [90] and Daoudi et al. [91] used a different approach to measure the elasticity of a material by use of AO.

A high intensity US burst is focused into the object on the region of interest. Inside the focus a shear wave is generated which radiates away from the focal point with a speed of typically 1-2 mm/ms which depends on the viscoelastic properties of the medium. This low speed causes a speckle decorrelation on ms time scale in transverse direction. This technique has a lateral resolution in the order of mm and is not limited to use at the surface. Li et al. [92] showed that by using the acoustic radiation force the resolution of a measurement can be increased by 40% to 110%.

Sing et al. [93] used two transducers which caused a beat and shear wave frequency of 250 Hz. This low frequency shear wave was detectable with a speckle contrast measurement.

2.6.4 Acousto-optic assisted light focusing in turbid media

Xu et al. [94] presented another detection technique called time-reversed ultrasonically encoded (TRUE) optical focusing based of a PRC used as a phase-conjugate mirror. The setup uses 3 arms, one signal arm where the object is located, and two reference arms. The first reference arm is used for the creation of the hologram inside the PRC, the second illuminates the crystal from the opposite direction. By the hologram inside the crystal the light is focused inside the object with the focal point inside the US focus region. This increases the local fluence at the US focus; in the future one can expect a significant improvement of the light level at the focus if the phase conjugate mirror exhibits a noticeable gain. This method makes AO the only technique that can create a guide star, which makes direct focusing of light possible in turbid media. Inside the US focus this light is tagged and detected outside the medium. A second benefit from using this phase conjugate PRC setup is the improved spatial resolution with a factor of $\sqrt{2}$. The disadvantage of using a PRC is that the hologram is destroyed when high gain factors are required. By using a spatial light modulator Tay et al. [95] where able to focus more light trough the US focus because the hologram on the SLM doesn't get destroyed.

Judkewitz et al. [96] improved the spatial resolution by focusing on only one speckle in the ultrasound focus. They call this method TROVE time reversal of variance-encoded light. They showed a lateral resolution of approximately 5µm.

2.6.5 Ex vivo and in vivo experiments

Various groups report measurements *ex* and *in vivo* with the use of AO.

Kim et al. [19] showed an image of chicken breast tissue with an embedded methylene-blue-dyed sentinel lymph node. Another *ex vivo* measurement on chicken breast is performed by Hisaka and Sasakura [97], they also used a reflection mode AO setup. Both experiments show the feasibility of a reflection mode AO setup on real tissue.

Kothapalli and Wang [98] embedded mouse and rat blood vessels in tissue mimicking phantom material at a depth of 3 mm and imaged these vessels with an AO microscopy setup. They also tested the AO microscopy setup on a phantom [99]. These experiments where performed *ex vivo* and

show the possibility of measurements on tissue and have thus the correct scattering and absorption coefficients. Recently Lai et al.[100] showed an *ex vivo* measurement on an HIFU induced lesion and compared the result with B-mode ultrasound. They concluded that AO sensing can follow the formation of the induced lesion in real time and for noncavitating lesions AO gives a more robust signal compared with B-mode ultrasound. Murray et al. [101] further investigated the changes in AO response of ex vivo chicken breast while elicited by a high-intensity ultrasound field. They concluded that with the use of AO it is possible to probe in real time the formation of a HIFU lesion.

In vivo experiments are performed by Lev et al. [102, 103]. They demonstrate that *ex vivo* measurements suffer much less from speckle decorrelation than *in vivo* experiments. Further they demonstrated the first AO tomography measurements on both mice and humans.

2.7 Discussion and outlook

Tagged photons can be detected with several techniques. The photodetectors which are fast enough to match the frequency of the US have, in general, small detector surfaces. To avoid loss of SNR, averaging over multiple speckles must be avoided. These properties lead to a small *etendue* and thus a low count of tagged photons. CCD arrays can detect light from thousands of speckles in parallel and collect more light, resulting in an expected higher SNR. Unfortunately these detectors are slow, therefore a lock-in detection is used and only a few phases of the US are sampled.

Compared to untagged photons, tagged photons have a shifted optical frequency. Several spectrometer based techniques are described in literature and have the advantage of greater stability. Small fluctuations in power, wavelength and phase are canceled out assuming a long coherence length of the laser light. By using heterodyne detection it is possible to distinguish between speckle decorrelation by Brownian motion, shot-noise level and the signal strength. Heterodyne detection also amplifies the signal optically to rise the signal above the level of the untagged photons.

PRC based detection has a large *etendue* and the advantage of signal amplification. The disadvantage is the low response time of typical crystals, which makes it sensitive to speckle decorrelation. Spectral hole burning or confocal Fabry-Perot filters are insensitive to speckle decorrelation because they act as bandpass filters and have the largest *etendue* [63]. Crystal must be cryogenically cooled in order to achieve a narrow bandwidth in the MHz range and Fabry-Perot need to be stabilized

with a high precision feedback loop and isolated from mechanical vibrations.

To achieve high resolution in lateral direction an ultrasound transducer with a small focal spot size is required. To achieve good axial resolution the frequency, phase and/or amplitude of the ultrasound can be made time dependent. This way only in a small part of the column, defined by the US beam, the light is tagged with these specific properties. The main advantage of giving a short US burst (amplitude) is the high acoustic peak pressure and therefore large modulation of light. The advantage of giving a chirped US pulse is the amount of information that is received in a single measurement; instead of measuring a single point, information can be extracted along the line in the US propagation direction.

The major challenges in *in vivo* AO applications are speckle decorrelation and low light levels. In general a detection method that detects as many tagged photons as possible is desired to obtain a good SNR. One strategy would be longer integration times, however *in vivo* speckle decorrelation occurs on time scales of 1 ms. Most PRC have a response time orders of magnitude longer than 1 ms and are therefore not suitable for *in vivo* measurements. CCD based techniques must acquire all light within the speckle decorrelation time, increasing shot noise and decreasing SNR. Spectral hole burning and Fabry-Perot interferometers are insensitive for speckle decorrelation and thus has none of these disadvantages however it is difficult to make sufficiently large etendue. Therefore these techniques are likely to be most suitable for *in vivo* imaging. Another more fundamental aspect in the introduction of acousto-optics for *in vivo* application is the uncertainty regarding the exact information that is provided by AO. Although the spatial resolution of AO is potentially good, the property that it samples is related to the local fluence rate which usually exhibits variations over a larger spatial scale. This aspect can be investigated using the new technologies that have been described in this review.

3 Towards acousto-optic tissue imaging with nanosecond laser pulses

Abstract[2]

We present a way to generate acousto-optical signals in tissue-like media with nanosecond laser pulses. Our method is based on recording and analyzing speckle patterns formed by interaction of nanosecond laser pulses with tissue, without and with simultaneous application of ultrasound. Stroboscopic application allows visualizing the temporal behavior of speckles while the ultrasound is propagating through the medium. We investigate two ways of quantifying the acousto-optic effect, viz. adding and subtracting speckle patterns obtained at various ultrasound phases. Both methods are compared with the existing speckle contrast method using a 2D scan and are found to perform similarly. Our method gives outlook on overcoming the speckle decorrelation problem in acousto-optics, and therefore brings in-vivo acousto-optic measurements one step closer. Furthermore it enables combining acousto-optics and photoacoustics in one setup with a single laser.

3.1 Introduction

Two hybrid techniques that combine optical contrast and the relatively high resolution of ultrasound (US) in turbid media are photoacoustics (PA) and acousto-optics (AO). [17, 104] Both methods can be combined to achieve fluence compensated PA imaging[7, 8]. While PA already has in vivo applications, AO still suffers from so called speckle decorrelation

[2] This chapter is published as: S. G. Resink, E. Hondebrink, and W. Steenbergen, "Towards acousto-optic tissue imaging with nanosecond laser pulses", Optics Express 22, 3564 (2014).

when applied in vivo, which typically results in no or poor signals. AO imaging is performed by injecting coherent light into the sample. The light is scattered by the sample and the exiting light forms a speckle pattern. By applying focused ultrasound on the sample the light acquires a modulated phase change in the US focus.[27] This results in a modulated speckle pattern with the frequency of the applied ultrasound (time scale ~ 1μs). The amount of modulation can be detected in several ways. Usually these methods require the measurement to be performed within the so-called speckle decorrelation time. Often cw lasers are used and chopped to generate relatively long pulses with long coherence length. Because of the low power a long integration time is necessary to integrate multiple pulses for different phases of the modulated speckle pattern. The total time to acquire one data point is close or even more than the speckle decorrelation time in tissue (~ 0.1 ms)[105], which impedes in vivo application. Here we demonstrate a novel method that brings us close to measuring acousto-optic signals far within the speckle decorrelation time of living tissue. To this end we use a laser that combines an adequately long coherence length with short (nanoseconds) high intensity pulses. In the eventual implementation of the method we will apply two nanosecond pulses within one ultrasound cycle. For now we use a laser at a repetition rate of 10 Hz, thus stable phantoms with long decorrelation time (>100 ms) are used to give a proof-of-principle.

3.2 Theory

Speckles are the result of interference of multiple randomly phased light waves. When the phases of these waves are modulated due to interaction of ultrasound with the medium, the intensity of the speckle is modulated. The modulation depth I_{ac} is associated with the optical and acoustical properties at the location of the ultrasound and the local fluence. The light waves that cause the intensity modulation are said to be 'tagged' by the ultrasound. The associated intensity to this tagged light is I_t where the non-tagged light has an intensity of I_{nt} and the total light illuminating a CCD pixel n at time t can under assumption of the absence of higher harmonics be approximated by:

$$I(n,t) = I_{dc}(n) + I_{ac}(n)\cos(\omega t + \varphi(n)) \tag{3.1}$$

Where $I_{dc}(n) = I_{nt}(n) + I_t(n)$, $I_{ac}(n) = 2\sqrt{I_{nt}(n)I_t(n)}$, ω the ultrasound angular frequency and φ the random phase for pixel n, where for the time being we neglect higher harmonic signals. Here we want to demonstrate the use of a coherent ns pulsed laser in an AO application. We let this laser illuminate the scattering medium when a US burst reaches a region of interest inside that medium, at time t. A camera detects the generated speckle pattern I_1 at the opposite end of the medium for which we write

$$I_1(n) = I_{dc}(n) + I_{ac}\cos(\varphi(n)) \tag{3.2}$$

A small time difference Δt later a second laser pulse is injected in the sample. This time is chosen to be half the ultrasound period so that we have a phase shift of π. At that moment a second speckle pattern I_2 is recorded, where:

$$I_2(n) = I_{dc}(n) - I_{ac}\cos(\varphi(n)) \tag{3.3}$$

Both speckle patterns are normalized such that the average intensity over all pixels is unity. The difference of the speckle patterns becomes larger if relatively more light has interaction with the US. We define the acousto-optic signal S_{AO} that quantifies the amount of tagged light as

$$S_{AO} = \left\langle \left(I_1(n) - I_2(n)\right)^2 \right\rangle \tag{3.4}$$

Where <> denotes averaging over all pixels of the speckle pattern. It can be shown that S_{AO} is proportional to the amount of tagged light by substituting equations 3.2 and 3.3 in equation 3.4 and using the definition of I_{ac}. On substitution we obtain :

$$\left\langle \left(I_1(n) - I_2(n)\right)^2 \right\rangle \propto \left\langle I_{nt}(n) I_t(n) \right\rangle = \left\langle I_{nt}(n) \right\rangle \left\langle I_t(n) \right\rangle \tag{3.5}$$

Hence the mean square difference of the speckle patterns is proportional to the amount of tagged light. Because of the normalization and $\left\langle I_t(n) \right\rangle \ll \left\langle I_{nt}(n) \right\rangle$ we approximate $\left\langle I_{nt}(n) \right\rangle = 1$. The proportionality constant is not important for a proof of concept because signal and noise are then multiplied with the same number.

This method has some similarities with an earlier technique that uses chopped CW lasers, which however needed orders of magnitude more camera integration time than the few nanoseconds that we use [24]. We will derive equations 3.4 and 3.5 in more detail in a later paper and make it quantitative instead of just qualitative. The difference between the two consecutive speckle patterns is caused by the effect of the ultrasound, speckle dynamics due to internal motion in the medium, camera noise and shot noise. By recording a large number of speckles (~10^5) the noise is minimized and converges to a DC offset in the measured AO-signal. The DC component in the intensity of individual speckles cancels out.

Besides this difference-based method it is possible to include both light pulses in one camera exposure, which we refer to as the addition method. This results in one speckle pattern that is the sum of two

instantaneous speckle patterns. This pattern has a contrast difference ΔC compared to the contrast C_0 of a speckle pattern of one pulse. For this implementation, the reduction in contrast is regarded as our acousto-optic signal. The reduction in contrast ΔC is given by:

$$\Delta C = C_0 - C \tag{3.6}$$

and the contrast of the integrated speckle pattern C is given by the standard deviation of the speckle pattern over its average value. For the sum of two speckle patterns this becomes:

$$C = \frac{\left(\left\langle \left(I_1(n)+I_2(n)\right)^2 \right\rangle - \left\langle I_1(n)+I_2(n)\right\rangle^2\right)^{1/2}}{\left\langle I_1(n)+I_2(n)\right\rangle} \tag{3.7}$$

This method is a variation of the speckle contrast method [47] where we now use two short pulses of light instead of a continuous wave over an entire US cycle.

3.3 Materials and methods

For both types of signal generation we use the setup described in figure 3.1.

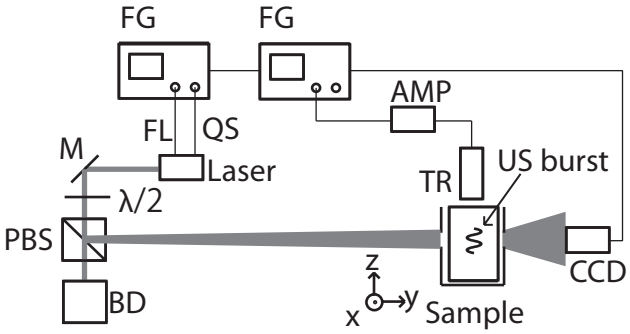

Figure 3.1. Experimental set-up. FG: function generators, AMP: amplifier, TR: Ultrasound transducer and BD: beam dump

The novelty is the use of a highly coherent short pulse laser. We used a frequency doubled injection seeded Nd:YAG laser (Newport Quanta Ray lab series 170) with pulse repetition rate 10 Hz, and Fourier limited pulses with a duration of 5ns, which results in a coherence length of 1.5 m and a pulse energy of 350mJ. This system is capable of delivering enough light in a single pulse to generate a speckle pattern at the camera after transmission through a turbid medium and the energy is also sufficient for

photoacoustic applications. Two synchronized function generators (FG)(Tektronix AFG 3102) give two TTL trigger signals for the laser consisting of flashlamp (FL) and Q-switch (QS) A third trigger is for the camera (CCD)(Allied Vision Technologies Manta G-145B NIR). At t=0 the flashlamp is triggered, the QS trigger at t=180 μs and the waveform for the US at ~162 μs depending on the depth of the ROI and the phase of the waveform. We use a simple setup for the delivery of the acoustics. The applied waveform is a sine at 5 MHz with 5 cycles. The waveform signal is amplified by ~50 dB by the amplifier (AMP) (Electronics & Innovation A075) and is connected to a focused 5 MHz US transducer (TR) (Olympus Panametrics-NDT V310). The laser light of 532 nm is attenuated with a half wave plate (λ/2) and a polarized beam splitter to reduce the pulse energy while operating the laser at its most stable settings. The excess light is collected by the beam dump (BD) so that the sample is illuminated with an optical pulse energy of approx. 3mJ. The repetition frequency of the laser is not high enough to give two pulses within one US cycle, thus we give a second US burst in time before the second laser pulse.

When the position of the US is shifted less than a wavelength the phase of the US is effectively changed. For the AO signal derived from the speckle pattern of two laser pulses the AO-signal strength depends on this phase difference. To show that the maximum signal is around π phase shift we perform a phase stepping experiment where we find the signal strength as function of the phase difference of the US bursts. Maintaining a π phase shift of the US between the two pulses of the laser it is possible to obtain an image by scanning the US focus through the object. We only use two phases for several reasons. Firstly it keeps the measurement time limited. But more importantly, in the eventual implementation we are will deliver 2 laser pulses within one US cycle, the current two phase measurement mimics this as close as possible. For the time being we need an object with tissue like properties with a longer speckle decorrelation time to overcome the problem of a low repetition rate of the laser. The phantom is a cylinder with a diameter of 20 mm and a length of 40 mm consisting of 3% agar and 3% Intralipid 20% without added background absorption. The background reduced scattering coefficient is estimated to be $\mu_s' = 0.6\ mm^{-1}$. We scanned in the plane perpendicular to the ultrasound propagation direction, which is in z direction. The optical axis runs parallel to the y-axis. The optodes at the opposite ends have a diameter of 3mm. Both the subtraction and addition method were applied at the same time from the same speckle patterns. For the addition method we need to determine C_0 for every data point, however this contrast value remains the same within a small variation during the whole experiment. Therefore we assume this value to be constant and it is only measured at the start of the experiment.

We performed a measurement on the same phantom in an acousto-optic setup based on speckle contrast and a CW laser with the same

experimental settings. Only the integration time of the camera is enlarged to 10 ms per speckle pattern to capture enough light, opposed to the effective 2 phases times 5ns=10 ns integration time in our novel method. We chopped the light from a CW laser (Coherent Verdi 6, 532nm) with the use of an acousto-optic modulator to obtain pulses of 1 μs. So we only tag light from the same region as in the other experiments. Within the 10 ms exposure time we send 250 acoustic and laser pulses to capture enough light. At the opposite end of the object we capture a speckle pattern with the camera. In this way we show the relation between AO-signals generated with the speckle contrast method and the proposed technique.

But before these experiments we performed a stroboscopic measurement on a very stable phantom to test the setup. With our system we obtained snapshots of a speckle pattern for different positions of the ultrasound. By varying the delay between light and sound delivery we stroboscopically recorded the evolution of the speckle pattern while the US travels through the medium. The ultrasound traveled along the z-axis and we placed the origin of this axis at the US focus. This experiment took several minutes and we wanted the speckle pattern to return to its original shape. This required a very stable sample material. We performed this experiment with a very stable homogeneous 5% agar phantom with paper particles of size ~300 μm as scatterers. The dimensions where the same as previously described phantom. We used the bigger paper particles in a more rigid agar matrix to maximize the decorrelation time of the speckle pattern. Brownian motion and thus speckle decorrelation is particle size dependent and the bigger scatterers result in the sample result in a decorrelation time of 10 minutes (speckle pattern cross correlation reduced to ~90%).

3.4 Results

The results of our stroboscopic measurement where we follow the blinking of many speckles at once are shown in figure 3.2.

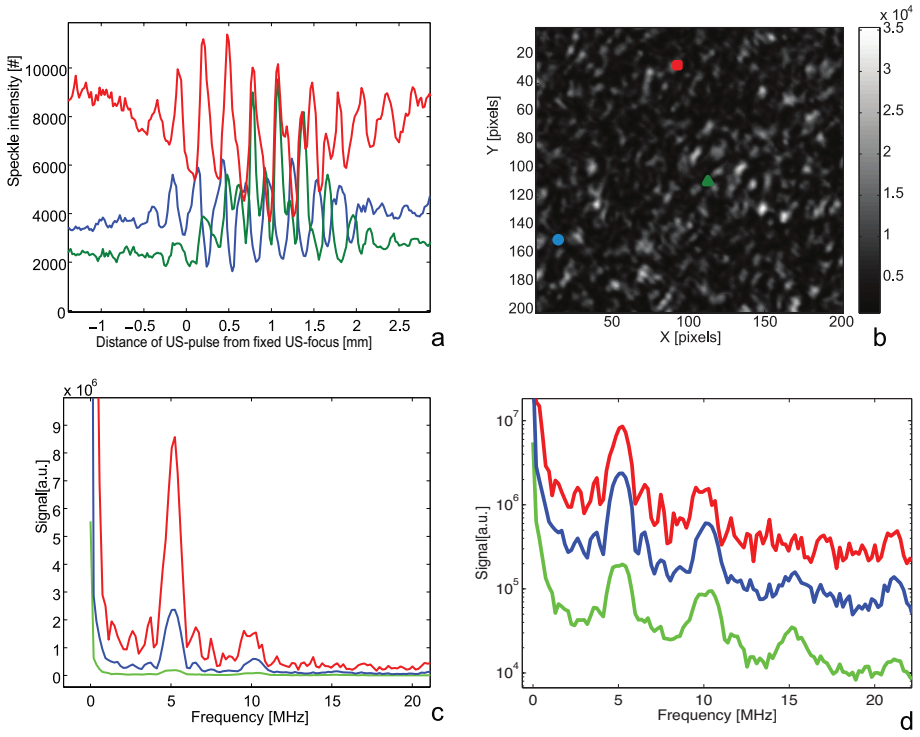

Figure 3.2. (a) The intensity modulation of three randomly chosen speckles (location in b indicated by line color) as function of z-position of the US burst from the fixed US focus (b) speckle pattern and frame from the attached mov-file where the color scale is optimized for print. (c, d) The average power spectrum of the modulation for 3 groups of speckles: low, average and high intensity. The red (square/ upper lines) denotes a bright speckle; Blue (circle/ middle lines) denotes a speckle with average brightness. Green (Triangle/lower lines) denotes a dark speckle.

The blinking of 3 speckles, as specified in figure 3.2(b) when the US interacts with the light is shown in figure 3.2(a) and the attached mov-file. This visualizes, to our best knowledge, for the first time the modulation of a speckle pattern while ultrasound propagates through a scattering medium opposed to following a single speckle in real-time i.e. [14, 15]. The integration time for a single speckle pattern was ~5 ns. Figure 3.2(c) and 3.2(d) show power spectra for the blinking of 3 categories of speckles. We observe that the ratio between the 5 MHz (US frequency) signal amplitude and the 10 MHz (first harmonic) signal amplitude depends on the brightness of the speckle. The brightest speckle has a ratio of ~5.7, the intermediate 4.0 and the dark speckles 2.2. We see that the phase of a speckle intensity signal is randomly related (figure 3.2(a)) to that of the US. We expect that sets of two speckle patterns with the biggest mutual

differences are found at opposite phases of the ultrasound, suggesting that a π phase shift is optimal for acousto-optic signal generation. We tested this with a phase stepping experiment in which by varying the delay of the US we varied the phase difference from 0 to 2π. The normalized AO-signal amplitude from the difference method is plotted in figure 3.3 for the whole range of phase differences.

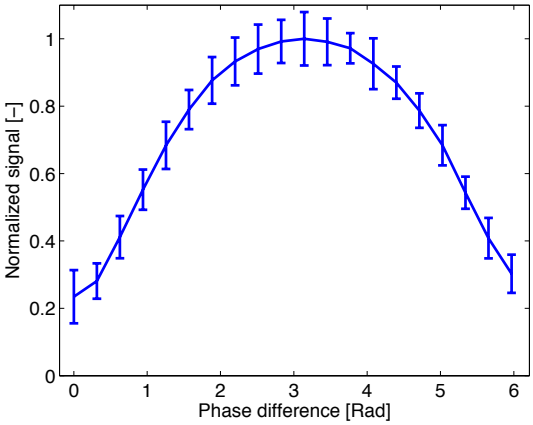

Figure 3.3. Normalized AO-signal as function of US phase difference as acquired using the speckle pattern subtraction method. The size of the error bar denotes the standard deviation on the raw AO-signal. The line connects the average values for all realized phase differences.

We scanned our homogeneous 3% agar phantom 6 times, and for each scan we calculated the AO-signal and took the median for both methods to reduce the effects of noise. We scanned the plane perpendicular to the US propagation at a depth of 23 mm or approximately 0.88 inch where the transducer is focused and from light injection aperture to detection aperture. This result was verified with a speckle contrast AO measurement. The results of the three methods are shown in figure 3.4. Figure 3.5(a) gives a pixel-by-pixel comparison of the three images in figure 3.4 and figure 3.5(b) shows the subtraction method versus the addition method.

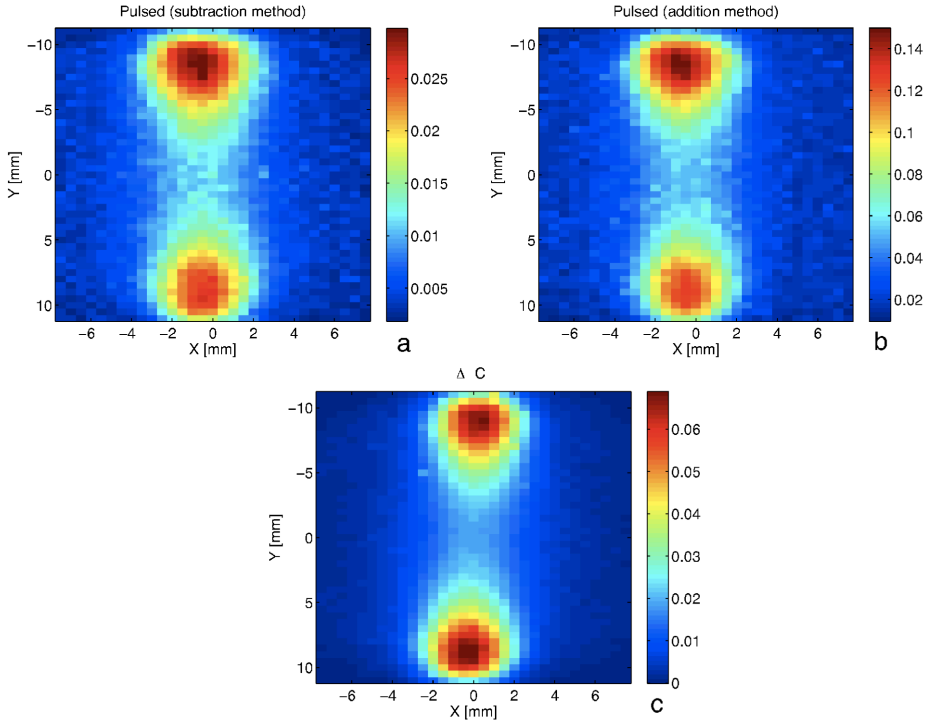

Figure 3.4. AO scan results for subtracting two speckle patterns (a), adding two patterns (b) and speckle contrast method (c).

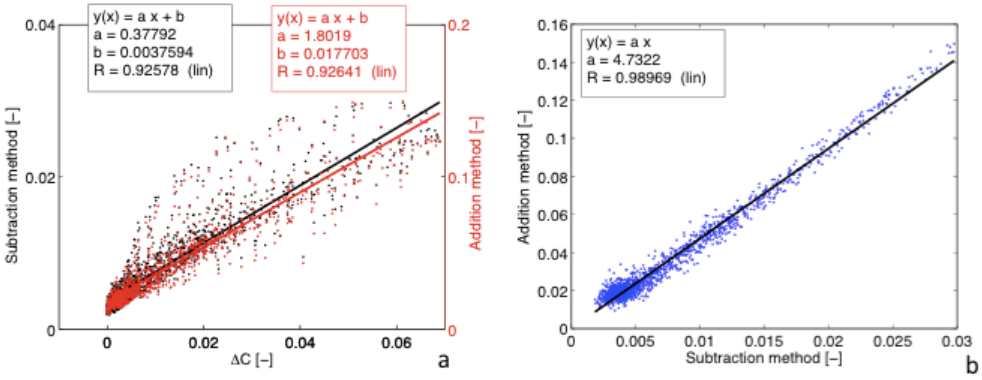

Figure 3.5. Comparison of (a) pulsed methods vs. speckle contrast in CW setup, and (b) the addition method vs. subtraction method. The AO-signal from subtracting patterns (black, left axis) and addition of patterns (red, right axis).

3.5 Discussion and conclusions

The above experiments show that it is possible to obtain AO-signals with a ns pulsed laser. For this we used an injection seeded Nd:YAG laser with Fourier limited pulse, implying a coherence length of 1.5 m. First of all, with the used laser it is possible to generate speckles through a 2 cm thick scattering sample with a contrast of 0.43 when both polarizations are allowed on the camera. This implies that the coherence length of the pulsed laser is sufficient. The stroboscopic measurement (figure 3.2) also shows that pulse to pulse no big mode hops or other beam instabilities are observed that would lead to different speckle patterns between pulses. All the speckle patterns for which no US is applied are virtually the same. We see that both bright and dark speckles contribute to the AO-signal, and that the bright speckles show more modulation (figure 3.2(a)). The relative amount of higher harmonics in the speckle intensity modulation depends on the brightness as well (figure 3.2(c)). This can be understood by taking the extreme case of a zero intensity region in the speckle pattern due to destructive interference: a modulation of part of the light by frequency ω will result in a 2ω frequency of the associated intensity variation since during each US cycle the local intensity will go from a minimum value (zero) to a maximum value twice. On the other hand, the brightest observed speckle is far from the maximum brightness possible, since in that case all the available energy goes into this single speckle, leaving the rest of space dark. And it is only this maximum possible intensity speckle that only can become less bright and might give higher harmonics.

The AO-signal strength depends on the US phase difference between the moments of illumination of the sample by the laser pulses. The maximum AO-signal is obtained for a phase shift of π radians. (Figure 3.3) The phase stepping experiment also shows that the shift of the US pulse over 2π or 1 US cycle brings the AO-signal close to that of the 0 shift case but not entirely. This is because the shifted US burst which consists of 5 cycles only overlaps for 4 cycles with the original one. However this effect is small enough to be neglected when performing a scan.

The AO-signal strength as defined by equations 3.4 and 3.6 behaves spatially very similar to speckle contrast measurements as shown by the scans for both the subtraction as addition method. (Figure 3.4) Both results obtained with the pulsed light are spatially very similar (figure 3.4(a) and 4(b)). As for their quantitative agreement, in a pixel-by-pixel comparison we observe on average a factor of ~4.8 between the results of the two methods. (Figure 3.5) These scans are also similar compared with the speckle contrast method. (Figure 3.4(c) and 3.5(a)). A part of the 'noise' in figure 3.5(a) is caused by the slight tilt in the scan of figure 3.4(c).

The equivalence of results after addition or subtraction of speckle patterns initially is counter-intuitive but can be explained. (Figure 3.5(b)) The bigger the difference between speckle patterns and keeping the average intensity constant for both would result in a lower standard deviation and thus lower contrast value. The fact that the addition method scales linearly with the difference method brings a great opportunity. For in-vivo applications an AO-signal should be acquired within the speckle decorrelation time of less than 0.1ms. Using two laser pulses within one US period can prevent speckle decorrelation within a measurement, e.g. a time interval of 100 ns between the two pulses for a 5 MHz US burst. To temporally resolve the speckle patterns resulting from these two pulses an ultra high-speed camera or a correctly triggered camera with sufficient short dead time is needed with high enough resolution for averaging over speckles. These cameras are expensive and large making them less desirable for future application. The addition method is equivalent to letting the camera integrate over two laser pulses. In the case of the addition method a relatively cheap and slow camera system can be used even in the case when much higher US frequencies are used and thus much shorter time between laser pulses. We see this as an important step towards in-vivo applications. To make this work we need to inject two laser pulses with sufficient wavefront matching, e.g. by splitting off light to a properly designed optical delay line. The properties of the used laser such as pulse duration and energy enable a combined performance of acousto-optic and photoacoustic measurements.

4 Solving the speckle decorrelation challenge in acousto-optic sensing using tandem nanosecond pulses within the ultrasound period

Abstract[3]

We present a novel acousto-optic (AO) method based on a nanosecond laser system, which will enable us to obtain AO signals in liquid turbid media. By diverting part of the light in a delay line we inject tandem pulses with 27ns separation. The change of the speckle pattern caused by the ultrasound phase shift reduces the speckle contrast of the integrated speckle pattern captured in a single camera frame. With these tandem pulses we were able to perform AO on a 2cm liquid turbid medium in transmission mode. We show the raw signal and a spatial AO scan of a homogenous water-intralipid sample. This approach is potentially capable of AO probing in-vivo since the acquisition time of approx. 40ns is 4 orders of magnitude less than the typical time scales of speckle decorrelation found in-vivo. The method may eventually enable us to

[3] This chapter is published as: S. Resink, E. Hondebrink and W. Steenbergen, "Solving the speckle decorrelation challenge in acousto-optic sensing using tandem nanosecond pulses within the ultrasound period", Optics Letters, Vol. **39**, Issue 22, pp. 6486-6489 (2014).

obtain fluence compensated photoacoustic signals generated by the same laser.

4.1 Introduction

Photoacoustic (PA) imaging currently finds many in vivo applications where the optical absorption delivers the contrast. A major challenge towards quantification of optical absorption is to compensate the signal strength of photoacoustics for local fluence variations. Recently fluence compensation of PA signals was proposed by using acousto-optic (AO) imaging[17, 104] in combination with PA[7]. This method relies on the principle that both PA and AO signal strength depend on the local fluence. The fluence dependency cancels out when the PA signals are normalized by the AO signal.

To enable biomedical use, both PA and AO must work in living, dynamic tissues. While this is not a problem for PA, for AO tissue dynamics has impeded practical in vivo application based on spatial speckle analysis. AO detection is based on either analysis of dynamic laser speckles or narrow band spectral filters like spectral hole burning [69] and Fabry Perot etalons[50]. The speckle based techniques are widely used but suffer from speckle decorrelation, leading to long measurement times and low signal-to-noise ratios. Ideally, a single AO measurement must be completed within the speckle decorrelation time. The rule of thumb is that in tissues the speckle decorrelation time is less than 1 ms[1] or even less than 0.1ms[105].

Recently we showed the usability of high intensity nanosecond pulsed lasers for AO signal generation [106] without the need of integrating over many pulses as in other nanosecond pulsed AO methods i.e. [96]. For overcoming stochastic variations in speckle contrast some averaging is beneficial. The use of nanosecond pulses has two benefits: First of all a pulsed laser easily delivers enough light within the speckle decorrelation time, so a bright speckle pattern of high contrast can be generated if allowed by the laser line width. Secondly, nanosecond pulsed lasers are compatible with photoacoustics where this type of laser is typically used. While our previous method could only be applied in media with a decorrelation time much larger than the pulse interval time(often 50-100ms) here we present a method that enables acquisition of an acousto-optic signal in scattering liquid samples in approx. 40 nanoseconds, hence far within the speckle decorrelation time of highly scattering liquids and biological tissues. This will enable in future in vivo fluence compensated photoacoustic imaging by adding acousto-optic probing using the same laser.

4.2 Materials and methods

In speckle based methods for acousto-optic tissue probing the ultrasound mediated intensity modulation of one or more speckles is used. The speckle intensity is modulated with mainly the ultrasound frequency. The fraction of the light that shows this modulation is said to be 'tagged' or 'labeled' by ultrasound. For small modulation this fraction is equal to the reduction in contrast.[47] Our recently presented method of AO signal detection [106] uses two pulses of several nanoseconds, each at a different phase of the ultrasound, such that the speckle pattern generated by the second pulse is slightly altered by the changed ultrasound interaction with the medium, compared to the first speckle pattern. Both speckle patterns were captured in two consecutive camera frames, and the acousto-optic effect was measured by either adding both images and taking the speckle contrast reduction, or by subtracting them, and taking the standard deviation. In the concept presented here we inject two laser pulses with only tens of nanoseconds separation. On this time scale there is virtually no speckle decorrelation, e.g. by Brownian motion or particle flow. The two pulses create two speckle patterns I1 and I2 for which we can write

$$I_i = \langle I_i \rangle + \Delta_i \tag{4.1}$$

where < > denotes spatial averaging over the detector surface and Δ_i a spatial perturbation from that average. Both patterns are normalized with $\langle I_i \rangle$ such that their average values are unity, hence

$$I_i = 1 + \Delta_i \tag{4.2}$$

The speckle contrast C is defined as

$$C = \frac{\sigma}{\langle I \rangle} \tag{4.3}$$

where σ is the standard deviation and $\langle I \rangle$ the average value of the intensity of the speckle pattern. The theoretical maximum value for the speckle contrast is 1 but several aspects are lowering the contrast of observed speckle patterns, such as the finite camera pixel size, the presence of two polarizations and camera noise. For the maximum speckle contrast that can be obtained with this setup from a single laser pulse we write

$$C_i^2 = \langle \Delta_i^2 \rangle = C_{\max}^2 \tag{4.4}$$

The camera adds the two speckle patterns in one exposure. Using equations 4.2 and 4.4 the resulting speckle contrast is calculated as

$$\begin{aligned} C_{sum}^2 &= \frac{\left\langle \left(I_1 + I_2\right)^2 \right\rangle}{4} - 1 \\ &= \tfrac{1}{4}\left(\left\langle \Delta_1^2 \right\rangle + \left\langle \Delta_2^2 \right\rangle\right) + \tfrac{1}{2}\left\langle \Delta_1 \Delta_2 \right\rangle = \tfrac{1}{2} C_{\max}^2 + \tfrac{1}{2} X \end{aligned} \tag{4.5}$$

with $X = \left\langle \Delta_1 \Delta_2 \right\rangle$. The lower this correlation the lower the speckle contrast, and two independent speckle patterns give $X = 0$ and $C_{sum} = C_{\max} / \sqrt{2}$. The quantity that we use for quantifying the acousto-optic effect is the normalized reduction in speckle contrast.

$$\Delta C_{norm} \equiv \frac{C_{\max} - C_{sum}}{C_{\max}} \tag{4.6}$$

Substituting equation 4.5 and rewriting equation 4.6 we obtain

$$\Delta C_{norm} = 1 - \sqrt{\tfrac{1}{2} + \frac{X}{2C_{\max}^2}} \tag{4.7}$$

A Taylor expansion of equation 4.7 around $X / C_{\max}^2 = 1$ gives

$$\Delta C_{norm} \approx \frac{1}{4} - \frac{X}{4C_{\max}^2} \tag{4.8}$$

When both patterns are identical we have X = $C_{\max}^2$ making ΔC_{norm} zero. When the two initial speckle patterns slightly differ through the interaction of ultrasound with the medium the correlation X drops and ΔC_{norm} increases. This method is the contrast method [47] with two short light pulses at different phases of the ultrasound, instead of a quasi CW illumination.

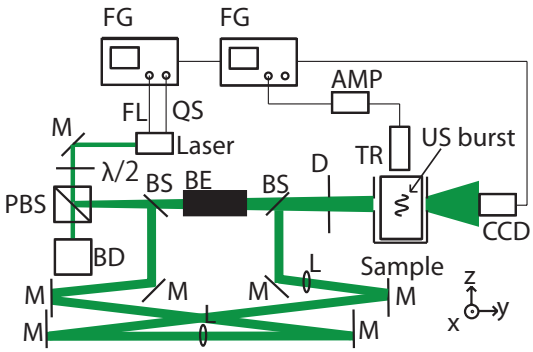

Figure 4.1. The experimental setup. FG: function generators, Amp: amplifier, FL: flash lamp trigger of laser, QS: Q-Switch trigger of laser, M: mirror, PBS: polarizing beam splitter, BS: 50:50 beamsplitter, TR: Ultrasound transducer, BE: Beam expander, D: Diaphragm and BD: beam dump and L: lens f=1000mm.

We use 532nm light of a frequency doubled injection seeded Nd:YAG laser with a pulse repetition rate of 10Hz and a pulse energy of 350mJ (Newport Quanta Ray lab series 170). The injection seeding of pulses with a duration of 5ns, results in a coherence length of 1.5m. The laser is triggered by two synchronized function generators (Tektronix AFG 3102) and its pulses are attenuated with a half wave plate and a polarizing beam splitter. This system delivers enough light in a single pulse to generate a bright speckle pattern at the CCD camera (Allied Vision Technologies Manta G-145B NIR) after transmission through a turbid medium. The laser beam is split into two arms with a 50:50 beam splitter. The short arm (30cm) leads to a second 50:50 beam splitter that is used as combiner, the second arm is extended with mirrors to achieve a total length of 8m. This length difference causes a pulse delay of 27ns. The measured dual pulse light intensity signal is shown in figure 4.2. The benefit of a tandem pulse vs. a long pulse is that all the light is only present at the extreme phases of the US. Further, a long pulse doesn't provide stress confinement for PA applications like a tandem pulse does with it small temporal features.

To compensate for beam divergence we placed two lenses (f=1000 mm) along the delay line.

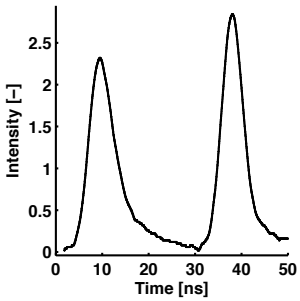

Figure 4.2. Temporal profile of the tandem pulse resulting from the 8m delay line, measured with a photodiode with a rise time less than 1ns.

Without ultrasound modulation, the speckle patterns generated by the direct and delayed pulses should be identical. This requires a large spatial coherence between the two pulses on the medium's surface. Due to the difference in propagation length from the laser cavity and the applied lenses the different curvatures of the phase fronts of both beams will compromise spatial coherence. To equalize the curvature of the phase fronts a beam expander (f=-30mm and f=75mm) is placed in the short arm. After the beam combiner a diaphragm (D=2mm) is placed for alignment purposes and improving the beam quality. The amount of light reaching the sample is approximately 3mJ per tandem pulse. We use our setup in transmission mode and the camera that captures the speckle patterns is placed 15cm behind the ∅3mm rear aperture of the sample. The wave fronts on the medium's surface of the fast and slow pulses must be very similar in curvature, angle and intensity distribution for this method to work. To test this, we compared the speckle pattern when only the short path is used with a speckle pattern when both paths are used. If the wave front curvature or intensity distribution is different the integrated speckle pattern will have a reduced contrast. When the angle of incidence is not matched properly then the long path light will generate a translated copy of the speckle pattern formed by the short path light for thin samples (the 'memory effect' [107]). These 'shifted' patterns are the input for the next thin layer of the sample, this also results in a lower contrast of the integrated speckle pattern.

4.3 Results

Figure 4.3 shows that the contrast for a speckle pattern by using only the short arm of the setup is 0.545, when both arms are used the resulting contrast is 0.528. This reduction of 3%, is sufficiently small because close to 90% of the potential maximum signal strength (which is a contrast reduction from 0.5 to 0.25) is still available. In other words the difference between zero signal and maximum signal is 12% smaller than optimal. Further, the speckle contrast reduction has a big stable component; only the

variation of the speckle contrast reduction is a source of noise in the measurement.

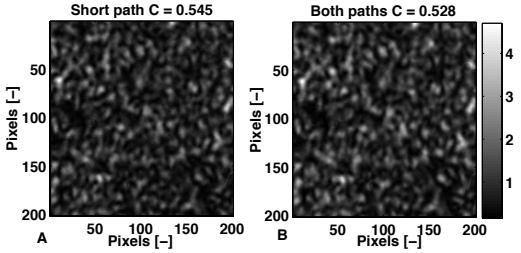

Figure 4.3. Normalized speckle patterns when only the short arm is used (A) and when both paths are used (B), for light transmitted through paper.

To create ultrasound modulation, the waveform from the function generator is a sine at 5MHz with 15 cycles. The waveform signal is amplified by ~50dB by the amplifier (Electronics & Innovation A075) whose output is connected to a focused (f=22.3mm, D_{focus}=1.1mm) 5MHz US transducer (Olympus Panametrics-NDT V310).

The sample consists of a 20mm diameter cylinder that is filled with a homogeneous mixture of 3% intralipid 20% ($\mu s' \approx 5$ cm^{-1})and water. Based on [108] we estimate the speckle decorrelation time to be approximately 25μs.

In a first experiment we toggle between an US 'on' and US 'off' state. The speckle contrast reduction (ΔC_{norm}) relative to a reference speckle pattern captured at the start of the experiment is plotted.

In a second experiment we perform a scan through the same homogeneous sample to obtain the so called banana shape that is the normalization parameter in sound light where fine structural information is obtained using PA. A focused US burst of 15 cycles scans the xy plane at the optical axis by mechanical translation at a step size of 0.5mm. The sample is illuminated by tandem pulses when the US burst intersects the xy plane.

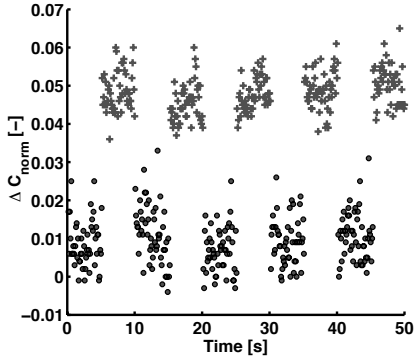

Figure 4.4. The raw acousto-optic signal obtained with the setup with US applied (+), interleaved with the background when no US is applied (o). Each image point is generated by one pulse pair separated by 27ns.

In figure 4.4 the raw AO signal is plotted when the sound is switched off and on 5 times. The signal during the US 'on' episodes is increased, hence the speckle contrast reduced. The average signal strength, defined as the difference of the averages in the 'on' and 'off' stages was 0.039 with an RMS value of 0.0066 during the off stages, hence the SNR we obtained was approximately 6.

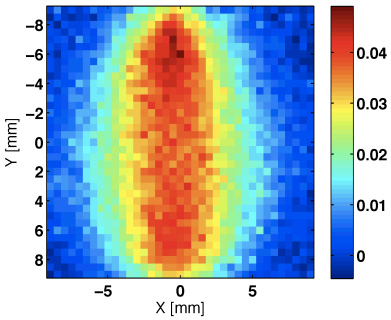

Figure 4.5. Distribution of ΔC_{norm} measured in the xy plane in a liquid scattering phantom.

In the second experiment the xy-distribution of ΔC_{norm} was measured 6 times and the median value is displayed in figure 4.5. The apertures for light injection and reception are at the top and bottom respectively. As expected, the signal strength along the optical axis was the highest and lower to the sides.

4.4 Discussion and conclusions

We clearly observe an acousto-optic signal with our setup in a 2cm liquid sample, with the AO signal obtained in 27ns only. Lev and Sfez. [103] measured an AO signal in a water-Intralipid mixture, based on the autocorrelation of the signal from a photomultiplier tube capturing the light of a single speckle. Their acquisition time was between 0.5-5 seconds. Assuming a speckle decorrelation time of 25µs they sampled approximately $2x10^4$ - $2x10^5$ statistically independent speckles within that acquisition time. This is roughly the same number as we sample in parallel with our camera in 27ns. Therefore we expect the same noise level but for a much shorter acquisition time. Other speckle pattern based methods like holography [54, 91] might be able to show better AO signals but require illumination over a full US cycle. Further, the fluences required for deep PA imaging might damage the acousto-optic modulators in the reference arm.

The AO scan shown in figure 4.5 clearly shows a 'banana shaped' radiance distribution of photons travelling from the injection to the exit aperture. The relatively low SNR of 6 has several causes. Firstly, the 27ns time delay between the two pulses is not optimal. The best delay time would be half the US period [106], or 100ns for 5MHz ultrasound, potentially leading to a fourfold increase in SNR. However a longer delay line would pick up more distortions from small density fluctuations in the air, extra mirror surfaces and lenses. Furthermore the imperfect spatial coherence of both pulses at the entrance plane reduces the signal. Without ultrasound both pulses should ideally generate exactly the same speckle pattern. However, when the wave fronts of both paths don't exactly match the speckle patterns are different. These small deviations from the ideal situation result in a lowered contrast of the combined speckle pattern. Additional changes induced by the US reduce the contrast less. The normalization with $C_{\max}$ corrects for this effect, however it amplifies both the noise and the signal. Therefore changes in the design of the delay line should aim for a higher spatial coherence between the two pulses along with a longer delay time.

The values in the scan displayed in figure 4.5 appear to be slightly lower than observed in the raw signal shown in figure 4.4. This is due to the use of a different reference speckle pattern and application of the median filter that removes the extreme values of the noise.

The presented method solves the challenges posed by speckle decorrelation in dynamic samples. Furthermore the pulse energy and pulse duration used here also allow for photoacoustic signal generation. The small time delay between the two light pulses ensures that only high frequency PA signals will be affected by the double pulse excitation. This

combined with the pulse energies of several mJ implies that this setup is also adequate for typical 1-5MHz PA signals. This is an important step towards in vivo fluence compensated photoacoustic imaging by adding acousto-optic probing using the same laser.

5 Tandem pulsed acousto-optics: an analytical framework of modulated high contrast speckle patterns.

Abstract[4]

Recently we presented acousto-optic (AO) probing of scattering media using addition or subtraction of speckle patterns due to tandem nanosecond pulses. Here we present a theoretical framework for ideal (polarized, noise free) speckle patterns with unity contrast that links ultrasound induced optical phase modulation, the fraction of light that is tagged by ultrasound, speckle contrast, mean square difference of speckle patterns and the contrast of the summation of speckle patterns acquired at different ultrasound phases. We derive the important relations from basic assumptions and definitions, which are then validated with simulations. For ultrasound-generated phase modulation angles below 0.7 rad (assuming uniform modulation), we are now able to relate speckle pattern statistics to the acousto-optic phase modulation. Hence our theory allows quantifying speckle observations in terms of the ultrasonically tagged fractions of light for near unity contrast speckle patterns.

---

[4] This chapter is published as: S. Resink, and W. Steenbergen, "Tandem pulsed acousto-optics: an analytical framework of modulated high contrast speckle patterns." Phys. Med. Biol. Vol. 60, pp. 4371(2015).

5.1 Introduction

Both photoacoustics and acousto-optic tomography [104] combine the use of light and sound in turbid media. Daoudi et al. [7] and Hussain et al. [8] demonstrated that the combination of both techniques makes it possible to perform fluence compensated photoacoustic measurements, opening the possibility of quantitative measurements of the optical absorption coefficient. In the underlying algorithm, the detected amount of ultrasonically tagged light is an important quantity. It would be ideal if both measurements can be done in the same setup, with the same laser system. This would give a more reliable method at lower costs, while increasing acquisition speed. However both techniques have different laser requirements. Photoacoustics (PA) needs short (typically ~5ns) high energy (>mJ) pulses and acousto-optics (AO) needs a long coherence length (>1m) and a temporal resolution that allows for recording the dynamic behavior of speckles under the influence of ultrasound. Traditionally acousto-optic measurements use a quasi CW laser so that a slow optical detector, often a CCD camera, can integrate over multiple US cycles. A camera is used for its high number of optical detector elements so that acquiring information for a great number of speckles is possible, thus increasing the SNR. [44]

Recently we have shown [106, 109] that it is possible to combine the important properties for PA and AO in one laser system, thus reducing the complexity of the system. One of these methods is the speckle contrast method [47]. A short laser pulse will give an instantaneous speckle pattern on the CCD and will thus have ideally a contrast of unity and will not give us any information on speckle dynamics. One option to perform a speckle contrast measurement is to integrate over a great number of short optical pulses each recorded at a different phase of the ultrasound. However in a dynamic medium like biological tissue this requires a high pulse rate. Recently we have shown that AO probing can be done with two nanosecond laser pulses each addressing a different phase of the ultrasound, where the speckle patterns due to each individual laser pulse are either subtracted or added. Here we investigate this new method and describe a way to quantify the signal such that the estimated amount of tagged light is comparable with the more traditional methods like speckle contrast that are well investigated [33, 47]. For clarity we show that the speckle contrast can be derived from the same equations as the AO signal in the sum and difference method that we presented in ref [106].

5.2 Theory

5.2.1 The relation between phase modulation and the tagged fraction

By applying ultrasound to a small tissue volume the light will be locally modulated by small index of refraction changes and scatterer displacements. The light is injected in the turbid medium and propagates along a great number of different paths through the medium. A part of these paths will overlap with the ultrasound and will be phase modulated. Here we restrict ourselves to linearly polarized speckle pattern. The electric field for a single polarization of path n can be written as

$$E_n = |E_n| e^{i\omega_l t} e^{i\left[\varphi_n + \delta_n \sin(\omega_{us} t + \phi_n)\right]} \tag{5.1}$$

where $|E_n|$ is the amplitude of the electric field, ω_l the oscillation frequency of the unmodulated electric field, t the time, φ_n is the phase of the light over path n at t=0 and δ_n is the phase modulation amplitude. The phase modulation has the frequency of the ultrasound $\omega_{us,}$ which for brevity will be denoted ω. This phase oscillation itself has a phase ϕ_n and is randomly distributed over the interval $(0,2\pi)$. When we investigate the influence of the phase modulation on the speckle pattern we can omit the fast oscillation of the electric field factor. The electric field then is described as:

$$E_n = |E_n| e^{i\left[\varphi_n + \delta_n \sin(\omega t + \phi_n)\right]} \tag{5.2}$$

When $\delta_n << 1$ we can write equation 5.2 as a sum of phasors as shown in figure 5.1: one static phasor that represents nontagged light and two phasors that rotate with the ultrasound frequency, one clockwise (c) and one anti-clockwise (a), leading to

$$E_n \approx |E_n| A_n e^{i\varphi_{0,n}} + \tfrac{1}{2}\delta_n |E_n| e^{i(\varphi_{c,n} - \omega t)} + \tfrac{1}{2}\delta_n |E_n| e^{i(\varphi_{a,n} + \omega t)} \tag{5.3}$$

where $|E_n| A_n$ is the amplitude of the stationary phasor. The phases $\varphi_{c,n}$ and $\varphi_{a,n}$ of the rotation of these phasors are chosen such that at $t=\tau_n$ the two rotating phasors are in line with each other and perpendicular to the stationary phasor, hence

$$\varphi_{c,n} - \omega\tau_n = \varphi_{a,n} + \omega\tau_n = \varphi_{0,n} + \tfrac{\pi}{2} \tag{5.4}$$

The fraction of light r_n that is tagged for this light path is then defined as the ratio of the energy of the tagged over the total amount of energy.

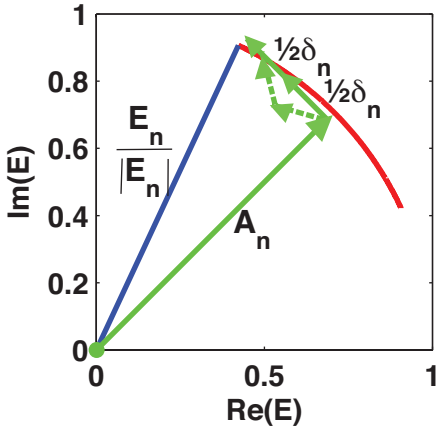

Figure 5.1. Phasor schematic for a unit length phasor E_n .In blue the phase modulated phasor and in green phasors representing the different terms from equation 5.3. The two counter rotating phasors have been depicted for two phases of the modulation.

Let us calculate the tagged fraction as a function of the phase modulation amplitude δ_n. The modulus of one rotating phasor (clockwise or anti-clockwise) is the square root of half the energy of the light that is tagged. The length of the stationary phasor A_n is the square root of the energy that is not tagged, which is related to the energy of tagged light by energy conservation. The phase modulation amplitude can then be approximated as:

$$\delta_n \approx \frac{\sqrt{\frac{1}{2}r_n}+\sqrt{\frac{1}{2}r_n}}{A_n} = \frac{2\sqrt{\frac{1}{2}r_n}}{\sqrt{1-r_n}} \tag{5.5}$$

and solving for r_n gives:

$$r_n = \frac{\delta_n^2}{\delta_n^2+2} \approx \frac{\delta_n^2}{2} \tag{5.6}$$

The fraction of light that is considered tagged is the average value of r_n, since some light paths might be strongly phase modulated, while other

phasors remain stationary. Thus the average fraction of tagged light R is expressed as

$$R \equiv \langle r_n \rangle = \left\langle \frac{\delta_n^2}{\delta_n^2 + 2} \right\rangle \approx \tfrac{1}{2} \langle \delta_n^2 \rangle \tag{5.7}$$

We now have the relation between phase modulation and tagged fraction which will be used to derive the equations that will set the phase modulations for a given R in our simulations.

5.2.2 Modulation of speckle intensity by tagged light

Speckles are the result of the interference of n randomly phased electric fields $E_n(t)$. The intensity of a single speckle is given as

$$I(t) = E_{tot}(t) E_{tot}^*(t) = \left(\sum E_n(t) \right) \left(\sum E_n(t) \right)^* \tag{5.8}$$

where $E_{tot}(t)$ is the total electric field for the speckle which, with the help of equation 5.3 can be written as

$$\begin{aligned} E_{tot}(t) &= \sum E_n(t) \\ &= \sum |E_n| A_n e^{i\varphi_{0,n}} + \sum \tfrac{1}{2} \delta_n |E_n| e^{i(\varphi_{c,n} - \omega t)} + \sum \tfrac{1}{2} \delta_n |E_n| e^{i(\varphi_{a,n} + \omega t)} \\ &= E_0 + E_c e^{-i\omega t} + E_a e^{i\omega t} \end{aligned} \tag{5.9}$$

where E_0 is the sum of all stationary phasors, E_c and E_a are the result of the clockwise and anti-clockwise rotating phasors respectively. The terms E_0, E_c and E_a have statistics resulting from a random walk in the complex plane where the step size is given as $|E_n| A_n$, $\tfrac{1}{2}\delta_n |E_n|$ and $\tfrac{1}{2}\delta_n |E_n|$ respectively. The phase and magnitude of the resulting phasors is random because the phases of each of the initial phasors is also random due to the random paths the light travels in the sample. In the complex plane $E_{tot}(t)$ describes a ellipsoid with its principal axis under a random angle resulting from this process. The center of this ellipsoid is at E_0, the length of the major and minor axis are $|E_c+E_a|$ and $|E_c-E_a|$.

By substituting equation 5.9 in equation 5.8 we obtain

$$I(t) = I_{0\omega} + I_{1\omega}(t) + I_{2\omega}(t) \tag{5.10}$$

where

$$\begin{aligned} I_{0\omega} &= E_0 E_0^* + E_c E_c^* + E_a E_a^* \\ I_{1\omega}(t) &= E_0 E_c^* e^{i\omega t} + E_c E_0^* e^{-i\omega t} + E_0 E_a^* e^{-i\omega t} + E_a E_0^* e^{i\omega t} \\ I_{2\omega}(t) &= E_c E_a^* e^{i2\omega t} + E_a E_c^* e^{-i2\omega t} \end{aligned} \tag{5.11}$$

The second harmonic term appears as cross terms from E_a and E_c. The magnitude of $I_{2\omega}$ is small compared with $I_{1\omega}$ but has comparable amplitude to $E_c E_c^* + E_a E_a^*$ and will not be neglected yet. We now have an expression that gives us the intensity of a single speckle as function of time.

5.2.3 The effect of tagged light on the speckle contrast

The contrast of a speckle pattern is defined as

$$c \equiv \frac{\sigma}{\left\langle I(\vec{x}) \right\rangle_{\vec{x}}} = \sqrt{\frac{\left\langle I(\vec{x})^2 \right\rangle_{\vec{x}} - \left\langle I(\vec{x}) \right\rangle_{\vec{x}}^2}{\left\langle I(\vec{x}) \right\rangle_{\vec{x}}^2}} = \sqrt{\frac{\left\langle I(\vec{x})^2 \right\rangle_{\vec{x}}}{\left\langle I(\vec{x}) \right\rangle_{\vec{x}}^2} - 1} \tag{5.12}$$

where σ is the standard deviation of the speckle pattern with intensity distribution $I(\vec{x})$ and $\langle\ \rangle_{\vec{x}}$ is the spatial average operator, further denoted as $< >$.

We recognize in $I_{0\omega}$ as given by equation 5.11 the summation of 3 statistically independent speckle patterns that are stationary in time. The phase relation between E_0, E_c and E_a canceled out for $I_{0\omega}$. Further $I_{1\omega}$ and $I_{2\omega}$ are periodical over 2π and π respectively and with an average value of 0.

In the quasi-CW AO speckle contrast method the intensity is averaged over an integer number of ultrasound cycles, the contributions of the 2 dynamic terms in *I(t)* are therefore negligible. The speckle contrast becomes

$$c_{\text{model}}^2 = \frac{\left\langle \left(E_0E_0^* + E_cE_c^* + E_aE_a^*\right)^2 \right\rangle}{\left\langle E_0E_0^* + E_cE_c^* + E_aE_a^* \right\rangle^2} - 1 = \frac{\left\langle \left(I_0 + I_c + I_a\right)^2 \right\rangle}{\left\langle I_0 + I_c + I_a \right\rangle^2} - 1$$
$$= \frac{\left\langle I_0^2 \right\rangle + \left\langle I_c^2 \right\rangle + \left\langle I_a^2 \right\rangle + 2\left(\left\langle I_0I_c \right\rangle + \left\langle I_0I_a \right\rangle + \left\langle I_cI_a \right\rangle\right)}{\left\langle I_0 \right\rangle^2 + \left\langle I_c \right\rangle^2 + \left\langle I_a \right\rangle^2 + 2\left(\left\langle I_0 \right\rangle\left\langle I_c \right\rangle + \left\langle I_0 \right\rangle\left\langle I_a \right\rangle + \left\langle I_c \right\rangle\left\langle I_a \right\rangle\right)} - 1 \tag{5.13}$$

The relative contributions of I_0, I_c and I_a are determined by the tagged fraction R. The amount of tagged light is equally divided over I_c and I_a, the untagged light I_0 is the remaining part; thus when $I_{0\omega}$ is normalized:

$$\begin{aligned} \left\langle I_c \right\rangle &= \left\langle I_a \right\rangle = \tfrac{1}{2}R \\ \left\langle I_0 \right\rangle &= 1 - R \end{aligned} \tag{5.14}$$

For speckle patterns with a contrast of unity we are allowed to use:

$$\left\langle I^2 \right\rangle = 2\left\langle I \right\rangle^2 \tag{5.15}$$

and for uncorrelated speckle patterns we can use

$$\left\langle I_m I_n \right\rangle = \left\langle I_m \right\rangle\left\langle I_n \right\rangle \tag{5.16}$$

Combining equations 5.13, 5.14, 5.15 and 5.16 we obtain an expression that links the tagged fraction to the contrast for ideal speckle patterns integrated over an integer number of ultrasound cycles, for small fractions of tagged light,

$$c_{\text{model}} = \sqrt{\tfrac{3}{2}R^2 - 2R + 1} \tag{5.17}$$

Solving for R gives

$$R = \tfrac{2}{3} - \tfrac{1}{3}\sqrt{6c_{\text{model}}^2 - 2} \tag{5.18}$$

For R<<1 we obtain

$$R = 1 - c_{\text{model}} \tag{5.19}$$

Equation 5.19 is similar to the result from the calculations described in[47] for small tagged fractions and close to unity contrast situations. So

we have an equation describing the speckle contrast as function of the tagged fraction.

5.2.4 The AO difference method

In the difference method, instead of integrating the speckle pattern over an integer number of ultrasound cycles we use two short light pulses at opposite ultrasound phases. We obtain speckle pattern $I(\vec{x},0)$ at time t=0 and $I(\vec{x},\pi/\omega)$ at t=π/ω of which the differences are induced by the ultrasound. Both speckle patterns are normalized. In equations 5.10 and 5.11 there is a static background term $I_{0\omega}$ that thus does not change between these two speckle patterns. $I_{2\omega}$ is small and periodic with half the ultrasound period and doesn't contribute to the speckle differences. $I_{1\omega}$ has an opposite sign between the two speckle patterns and is thus maximally different.

Using equation 5.11 the speckle difference can be written as

$$\begin{aligned} I(\vec{x},0)-I(\vec{x},\pi/\omega) &= \left(E_{0\vec{x}}E_{c\vec{x}}^{*}+E_{c\vec{x}}E_{0\vec{x}}^{*}+E_{0\vec{x}}E_{a\vec{x}}^{*}+E_{a\vec{x}}E_{0\vec{x}}^{*}\right) \\ &\quad -\left(E_{0\vec{x}}E_{c\vec{x}}^{*}e^{i\pi}+E_{c\vec{x}}E_{0\vec{x}}^{*}e^{-i\pi}+E_{0\vec{x}}E_{a\vec{x}}^{*}e^{-i\pi}+E_{a\vec{x}}E_{0\vec{x}}^{*}e^{i\pi}\right) \\ &= 2\left(E_{0\vec{x}}E_{c\vec{x}}^{*}+E_{c\vec{x}}E_{0\vec{x}}^{*}+E_{0\vec{x}}E_{a\vec{x}}^{*}+E_{a\vec{x}}E_{0\vec{x}}^{*}\right) \\ &= 2\left(2\left|E_{0\vec{x}}\right|\left|E_{c\vec{x}}\right|\cos\left(\angle E_{0\vec{x}}-\angle E_{c\vec{x}}\right)+2\left|E_{0\vec{x}}\right|\left|E_{a\vec{x}}\right|\cos\left(\angle E_{0\vec{x}}-\angle E_{a\vec{x}}\right)\right) \\ &= 4\left|E_{0\vec{x}}\right|\left(\left|E_{c\vec{x}}\right|\cos\left(\angle E_{0\vec{x}}-\angle E_{c\vec{x}}\right)+\left|E_{a\vec{x}}\right|\cos\left(\angle E_{0\vec{x}}-\angle E_{a\vec{x}}\right)\right) \end{aligned} \tag{5.20}$$

We want to express the influence of the ultrasound as a single number instead of a complete spatial pattern. Therefore we want to perform spatial averaging, however the spatial average of equation 5.20 is zero. Let us investigate the mean square difference,

$$
\begin{aligned}
I(\vec{x},0)-I(\vec{x},\pi/\omega) &= \left\langle \left(4\left|E_{0\vec{x}}\right|\left(\left|E_{c\vec{x}}\right|\cos\left(\angle E_{0\vec{x}}-\angle E_{c\vec{x}}\right)+\left|E_{a\vec{x}}\right|\cos\left(\angle E_{0\vec{x}}-\angle E_{a\vec{x}}\right)\right)\right)^2 \right\rangle \\
&= \left\langle 16\left|E_{0\vec{x}}\right|^2\left(\left(\left|E_{c\vec{x}}\right|\cos\left(\angle E_{0\vec{x}}-\angle E_{c\vec{x}}\right)+\left|E_{a\vec{x}}\right|\cos\left(\angle E_{0\vec{x}}-\angle E_{a\vec{x}}\right)\right)\right)^2 \right\rangle \\
&= \left\langle 16\left|E_{0\vec{x}}\right|^2\begin{pmatrix}\left|E_{c\vec{x}}\right|^2\cos^2\left(\angle E_{0\vec{x}}-\angle E_{c\vec{x}}\right)+\left|E_{a\vec{x}}\right|^2\cos^2\left(\angle E_{0\vec{x}}-\angle E_{a\vec{x}}\right)\\ +2\left|E_{c\vec{x}}\right|\cos\left(\angle E_{0\vec{x}}-\angle E_{c\vec{x}}\right)\left|E_{a\vec{x}}\right|\cos\left(\angle E_{0\vec{x}}-\angle E_{a\vec{x}}\right)\end{pmatrix} \right\rangle \\
&= \left\langle 16\left|E_{0\vec{x}}\right|^2\begin{pmatrix}{I_{c\vec{x}}}^2\cos^2\left(\angle E_{0\vec{x}}-\angle E_{c\vec{x}}\right)+{I_{a\vec{x}}}^2\cos^2\left(\angle E_{0\vec{x}}-\angle E_{a\vec{x}}\right)\\ +2\left|E_{c\vec{x}}\right|\cos\left(\angle E_{0\vec{x}}-\angle E_{c\vec{x}}\right)\left|E_{a\vec{x}}\right|\cos\left(\angle E_{0\vec{x}}-\angle E_{a\vec{x}}\right)\end{pmatrix} \right\rangle
\end{aligned}
\tag{5.21}
$$

Now let the contributions for $I_{0,}$ I_c and I_a be defined as

$$
\begin{aligned}
\left\langle I_{0\vec{x}}\right\rangle_{\vec{x}} \Big/ \left\langle I_{\vec{x}}\right\rangle_{\vec{x}} &= 1-R \\
\left\langle I_{c\vec{x}}\right\rangle_{\vec{x}} \Big/ \left\langle I_{\vec{x}}\right\rangle_{\vec{x}} &= \left\langle I_{a\vec{x}}\right\rangle_{\vec{x}} \Big/ \left\langle I_{\vec{x}}\right\rangle_{\vec{x}} = \tfrac{1}{2}R
\end{aligned}
\tag{5.22}
$$

Further the cross term has a spatial average of zero, by substituting equation 5.22 in 5.21 we get the relation between the tagged fraction *R* and the mean square difference of 2 speckle patterns,

$$
\begin{aligned}
\left\langle \left(I(\vec{x},0)-I(\vec{x},\pi/\omega)\right)^2 \right\rangle_{\vec{x}} &= 16\left(1-R\right)\left(\tfrac{1}{4}R+\tfrac{1}{4}R\right) \\
&= 8\left(1-R\right)R \approx 8R
\end{aligned}
\tag{5.23}
$$

Solving for R gives:

$$
R = \tfrac{1}{2}-\tfrac{1}{4}\sqrt{4-\left\langle \left(I(\vec{x},0)-I(\vec{x},\pi/\omega)\right)^2 \right\rangle_{\vec{x}}}
\tag{5.24}
$$

This expression provides an estimate of the tagged fraction R from the difference between two instantaneous speckle patterns for opposite ultrasound phases.

5.3 Materials and methods

We test the relations given by equations 5.7, 5.18 and 5.24 on simulated speckle patterns with modulation. On the output optode of a sample we define 2500 wiggling phasors on random positions and with a random phase. The phase modulation of these phasors is simulated using equations 5.2 and 5.8. For each pixel of the simulated camera the distance and thus phase relation between pixel and the origin of all 2500 output positions of the optode is calculated. Then for each pixel we calculate the intensity associated with the sum of all the electric field components. This gives us one instantaneous speckle pattern. For the speckle contrast simulations we take 20 snapshots of the speckle pattern equally spaced over one ultrasound cycle. We vary the tagged fraction R from 0 to 0.8 and use random phase variation amplitudes δ_n chosen such that equation 5.7 is satisfied for several phase modulation distribution functions of δ_n. We test 8 scenarios which are plotted in figure 5.2. For each value of R and each distribution function a histogram is generated with 51 bins of δ_n for values between $-\pi$ and π. We fill each histogram with 2500 randomly chosen values for δ_n within the constraints of the distribution function we test. The color scale represents the amount of values of δ_n within that bin.

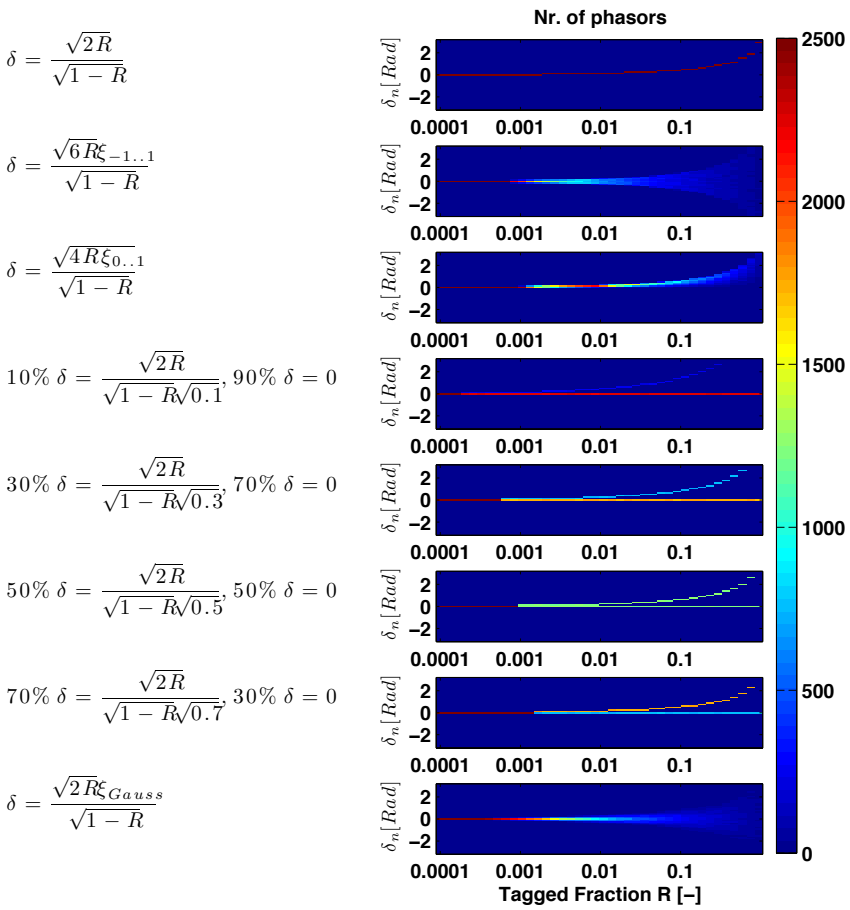

Figure 5.2. The different types of phase modulation distributions as function of R. Explanation is given in the main text.

Four classes of amplitude modulation distribution functions make up these 8 distributions. The first class has one phase modulation distribution and assumes all values for δ_n are equal and is shown in the first row of figure 5.2. The second class assumes a phase modulation distribution where all the modulation amplitude is randomly chosen between a lower and an upper limit. These distributions are designed such that the probability of finding a phase modulation is equal over the whole range or its square is equally distributed. These are shown in rows 2 and 3 of figure 5.2 respectively.

The third class assumes one part of all the light is not modulated and thus has cases in which $\delta_n = 0$. The remaining light is modulated with values for δ_n chosen equal. The modulated fractions of 10, 30, 50 and 70 percent are shown in rows 4, 5, 6 and 7 respectively.

For the fourth class of distributions we assume that the values of δ_n are distributed Gaussian. The distribution is shown in row 8 of figure 5.2. We expect the distribution to be more similar to that of class 3 when the tagging is close to the optodes. A fraction of the light can escape the medium without interacting with the ultrasound when the optode size is larger than the ultrasound focus. The Gaussian distribution might resemble a more realistic phase modulation distribution and we assume it resembles reality the best for most experiments. In the equations of figure 5.2, ξ denotes a random number: $\xi_{-1..1}$ is a random number from a evenly distributed set of numbers between -1 and 1, $\xi_{0..1}$ is evenly distributed between 0 and 1, and ξ_{gauss} is a Gaussian distribution with a standard deviation of 1 and an average of 0.

By using equation 5.2 we calculate the electric fields that form the speckle pattern. The light interferes on a virtual CCD array of 300x300 pixels that pointwise samples the speckle pattern. The average speckle size is 3 pixels resulting in approximately 10^4 speckles. To calculate the speckle contrast we add 20 instantaneous speckle patterns taken equally spread over one full US cycle to simulate integration on the camera over a finite time. The simulated speckle contrast is used to estimate the tagged fraction using equation 5.18.

The instantaneous speckle patterns of $t\omega = 0$ and $t\omega = \pi$ are stored for the two speckle patterns analysis. For the difference method we plot equation 5.24 as function of the set tagged fraction R that also determines δ_n via equation 5.7 for the simulated speckle patterns and compare this against equation 5.24.

5.4 Results

To illustrate the simulations we show speckle patterns for the 0 and π phase shift in figure 5.3 A and B respectively. The difference of both speckle patterns is plotted in figure 3 C, the blurred speckle pattern that is integrated over one ultrasound cycle is shown in figure 5.3 D. All the wiggling phasors have an identical phase modulation amplitude of 0.35 rad, leading to a tagged fraction R=0.058.

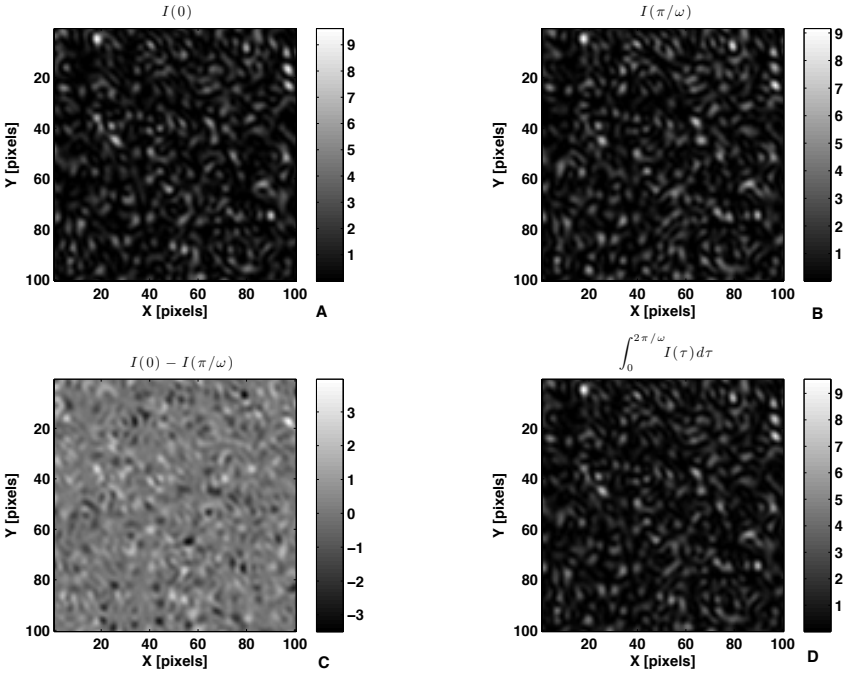

Figure 5.3. Cropped speckle patterns at phase 0 (A) and π (B), the difference of these (C) and the speckle pattern integrated over a full US cycle (D). The assumed tagged fraction was R=0.057.

For each phase modulation function the simulated tagged fraction was determined using equations 5.18 and 5.24 for the contrast and difference method for a range of set tagged fractions. For the Gaussian phase modulation distribution the results are plotted in figure 5.4.

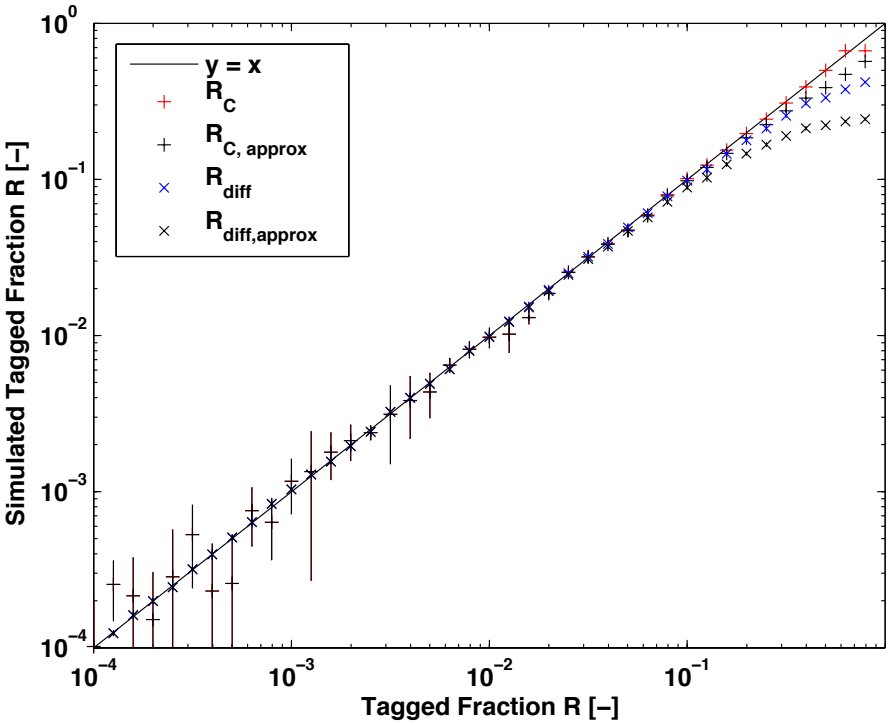

Figure 5.4. The simulation results based on a Gaussian distributed phase modulation amplitude. Here the simulated tagged fraction is shown for the contrast method (R_c, red +) and difference method (R_{diff}, blue x). The data that was obtained with the approximated versions of equation 5.19 and 5.23 ($R = \frac{1}{8}\left\langle \left(I(\vec{x},0) - I(\vec{x},\pi/\omega) \right)^2 \right\rangle_{\vec{x}}$) is given in black.

In figure 5.4 the simulated tagged fraction is plotted vs. the set tagged fraction. An ideal method would follow the line y=x. Both methods correctly predict the tagged fraction for values between 0 and 0.2 while the simplified methods represented by equation 5.19 and 5.23 only correctly predict R for a smaller range. For tagged fractions above 0.2, we see that both methods start to fail to reproduce the set tagged fraction. The contrast method performs better for high tagged fractions than the difference method. For the low tagged fractions the difference method is superior to the contrast method and shows much smaller statistical scatter. We test both methods for several distributions of phase modulation amplitudes that satisfy equation 5.7. The result is shown in figure 5.5 as fractional difference of the ideal behavior for the speckle contrast method (left) and the mean square difference method (right).

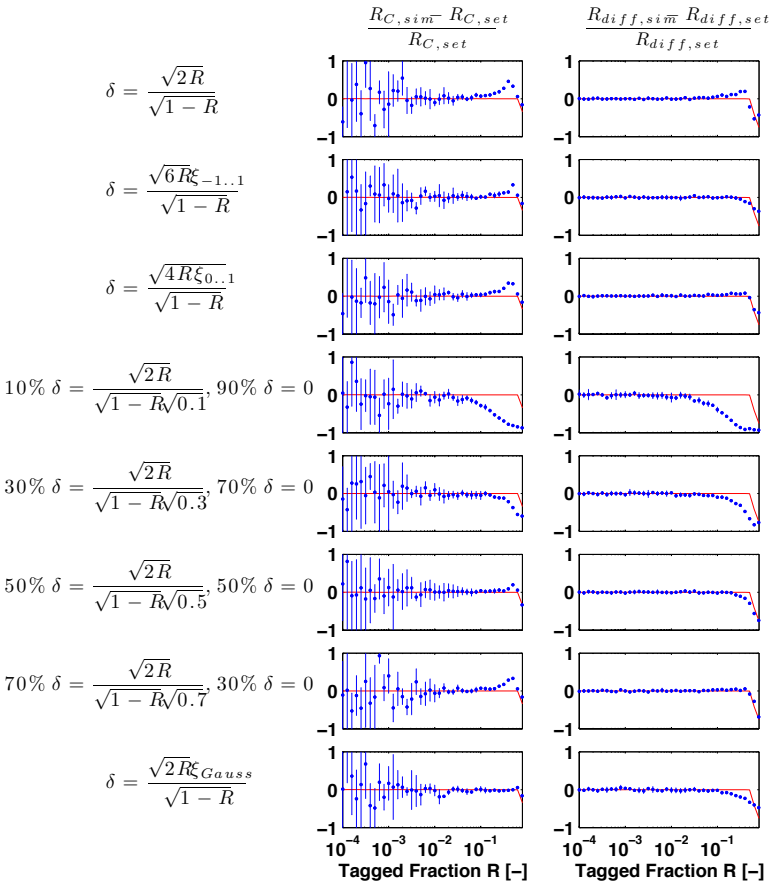

Figure 5.5. Fractional error in tagged fraction R for several phase modulation amplitude distributions. *Left* the contrast based method. *Right* the mean square difference. The y-axis resembles the relative deviation from the model: $\left(R_{simulated} - R_{set}\right)/R_{set}$.

The error bars depict the standard deviation over 15 simulations. The red line is calculated by substituting the result of equations 5.17 and 5.23 in equations 5.18 and 5.24. Equations 5.18 and 5.24 are the inverse of the parabolic equations 5.17 and 5.23 and are only valid for the lower values. This explains why the simulation results show a large underestimation of the set tagged fraction for the higher set values.

5.5 Discussion and conclusion

We have theoretically explored the relation between phase modulations of light and the resulting speckle pattern modulations. For a certain light trajectory, we modeled tagged light as two counter rotating phasors that are necessary to approximate a periodical phase modulation. The light represented by these rotating phasors is a fraction of the total light that forms the speckle pattern on the detector. This is the fraction of tagged light. The relation between the fraction of tagged light and the phase modulation is given in equation 5.7. We explored the effect of phase modulations on the difference between speckle patterns for a π rad ultrasound difference (difference method), and on the contrast of the speckle pattern integrated over a complete ultrasound cycle (contrast method). We showed the relation between the signal obtained with the difference method (equation 5.24) and speckle contrast method (equation 5.18) for ideal simulated speckle patterns. These relations were tested for simulated speckle patterns, with several phase modulation angle distributions. The analytical expressions allow for extraction of tagged fractions from speckle observations, and for simulated speckle patterns these predictions were show in agreement with the input values for fractions of tagged light upto 0.2. For very small fractions the error bars of especially the contrast method are large because of the stochastic properties of speckle patterns. The natural spread of speckle contrast is in the order of the contrast reduction caused by the phase modulation caused by the random nature of the speckle contrast[110]. Therefore the difference method is expected to perform better for small acousto-optic signals in experiments. The trend of the contrast method for low tagged fractions is however obeying the model. For larger fractions of tagged light R we often see an over or under estimation compared to the ideal behavior. This is because the assumption in equation 5.3 of small values for δ_n does not hold. A good example of this is given in the 4^{th} row of figure 5.5. In that case only a small fraction of all the light is modulated. That small fraction of light must be highly phase modulated to achieve the same amount of tagged light on the camera. When the phase modulation is large the counterrotating phasor model represented by equation 5.3 no longer holds. The simulation results depend on the phase modulation distribution, and we conclude that the model holds up to a tagged fraction of 20% for most tested distributions. The valid range of the model can be extended by making more accurate approximations and adding more terms to equation 5.3. However, in view of the simplicity of the counterrotating phasor model, the range of validity is remarkably large. When aiming for high signal strengths, tagged fractions R in the range 0.1-0.2 are associated with contrast values in the range 0.8-0.9 (according to equation 5.18), and hence reductions in contrast of approximately 10-20%. Such relative ΔC values have been observed in [106], which suggests that the theoretical

framework presented here will provide a valuable quantification framework for situations encountered in practice.

6 Tandem pulsed acousto-optics: obtaining the tagged light fraction from modulated non-ideal speckle patterns.

Abstract[5]

Recently we presented novel methods for acousto-optic (AO) imaging of biological tissues, taking 1) the mean square difference of speckle patterns (subtraction method) or 2) the contrast of the summation of speckle patterns (summation method) acquired from nanosecond pulses of coherent light, fired at different ultrasound phases. In this study we relate the two methods both analytically and experimentally. We experimentally show that these two methods are nearly identical provided that the maximum achievable speckle contrast is determined correctly. We show with simulations that after correction the outcome is independent of experimental detection parameters. This makes the AO methods in this study reliable, allowing quantifying speckle observations in terms of the ultrasonically tagged fractions of light. The use of tandem nanosecond

[5] This chapter is under review as: S. Resink and W. Steenbergen "Tandem pulsed acousto-optics: obtaining the tagged light fraction from modulated non-ideal speckle patterns" in Physics in medicine and biology.

pulses in one burst of ultrasound overcomes the challenge of tissue dynamics.

6.1 Introduction

Photoacoustics (PA) and acousto-optic tomography (AOT) [104] combine the use of sound and light in turbid media. The combination of PA and AOT measurements makes it possible to perform fluence compensated photoacoustic imaging as shown by Daoudi et al. [7] and Hussain *et al* [111]. In this approach, the so called ultrasonically modulated or 'tagged' fraction of light plays an important role. Ideally, the measurements are done with the same laser system; this reduces the costs, increases acquisition speed and gives more reliable results. However, these techniques have different laser requirements. PA needs short (typically ~5ns) high energy (>mJ) pulses while acousto-optics (AO) needs a long coherence length (>1m) and a temporal behavior that allows recording of the dynamic behavior of speckles under the influence of ultrasound. Recently we have shown the possibility to perform acousto-optic imaging with a laser system also suitable for photoacoustics [106], in a manner that overcomes the problem of tissue dynamics [109].

Acousto-optic measurements are usually performed using a quasi CW laser so that a camera, or other optical detector, can integrate over multiple US cycles. The cameras are used for their high number of optical detector elements and the increase in SNR that results from acquiring information from a great number of speckles [44].

One AO method that relies on a camera is the speckle contrast method [47]. However, we use a nanosecond laser pulse and therefore, no information on speckle dynamics is obtained within the laser pulse duration. The camera captures an unblurred speckle pattern that ideally has a unity contrast. However, it is possible to perform a speckle contrast measurement by integrating over multiple optical pulses applied in a range of ultrasound phases. In this study, we investigate two methods both experimentally and analytically: one is referred to as subtraction method while the second one is referred to as the summation method where two speckle patterns generated by nanosecond laser pulses are subtracted or added respectively. For these approaches, Resink et al. [112] recently presented a theoretical framework in the case of ideal speckle patterns with unity contrast. Here we present a theoretical framework to extract tagged fractions in case of non-ideal speckle patterns, hence with a background signal and noise, and compare this with the well known speckle contrast method. [33, 47]. Further we show that the data reproduces correct AO

values that are independent from the speckle contrast. This finding makes it possible to perform pulsed acousto-optics in a more quantitative way.

6.2 Theory

6.2.1 Relationship between the summation and subtraction methods in AO

Speckle pattern subtraction would require two separate speckle patterns to be recorded, either within one US cycle, or at least far within the speckle decorrelation time, e.g. using a high speed camera. However, by recording two speckle patterns within the same exposure of a slow camera it is possible to add instead of subtract the speckle patterns. This way the two laser pulses can be fired without inducing speed constraints on the used camera. Because of the US-induced changes in the speckle pattern, the sum of the two speckle patterns has a lower contrast than a singe speckle contrast. We call this procedure the summation method. The summation of the speckle patterns is similar to the speckle contrast method derived earlier [47, 112], except that the integration of light is now only carried out for two phases of the ultrasound instead of a continuum over 2π phases. In both summation and contrast method, the difference in contrast can be related to the tagged fraction. As shown by Resink et al. [112] (chapter 5) the temporal behavior of the intensity of the modulated speckles is described by

$$I(t) = I_0 + I_\omega(t) + I_{2\omega}(t) \tag{6.1}$$

with I_0 the static component, I_ω and $I_{2\omega}$ are dynamic and have a frequency of the US and twice that of the US respectively. The subtraction and summation methods each use different terms from equation 1. I_0 is static and thus would appear in a sum image twice. I_ω has an opposite sign at π phase and therefore this term cancels out on addition and does not contribute to the resultant signal of the addition method. The average value of $I_{2\omega}$ is zero and doesn't contribute to the average intensity. However, the standard deviation of $I_{2\omega}$ is non zero. Spatial averaging reduces the influence of $I_{2\omega}$ to 0 and is therefore ignored in the rest of our analysis. However the noise from this term will be visible in the signal, so the summation method is similar to the contrast method but not the same.

We want to adapt both methods for more realistic cases where the maximum speckle contrast is less than unity. In these cases the speckle contrast reduction is normalized with the maximum speckle contrast. This

method is also used in laser speckle contrast methods for perfusion imaging[113] to make results more comparable between different experiments and setups. How this correction influences the estimation of the tagged fraction is given in the next section.

In both the summation and subtraction method, two speckle patterns are recorded; one at phase 0: $I(\vec{x},0)$ the other at time π/ω: $I(\vec{x},\pi/\omega)$.

A speckle pattern $I(\vec{x},t)$ can be written as its average value $\langle I(\vec{x},t)\rangle$ plus a deviation $\Delta(\vec{x},t)$ from that average. For simplicity we assume the speckle patterns are normalized and thus the average value is unity, leading to

$$I(\vec{x},t) = 1 + \Delta(\vec{x},t) \tag{6.2}$$

The two speckle patterns are very similar but with small differences that are induced by the ultrasound. They can be written as

$$\begin{aligned} I(\vec{x},0) &= 1 + \Delta(\vec{x},0) \\ I(\vec{x},\pi/\omega) &= 1 + \Delta(\vec{x},\pi/\omega) = 1 + f(\Delta(\vec{x},0),\varepsilon) \end{aligned} \tag{6.3}$$

where $f(\Delta(\vec{x},t),\varepsilon)$ is an unknown function that gives $\Delta(\vec{x},\pi/\omega)$ as function of $\Delta(\vec{x},0)$ and small differences of the optical pathlengths ε induced by the ultrasound. The use of this function allows that some speckles become brighter and some darker and thus resembles the differences of a speckle pattern induced by the ultrasound. The properties of function $f(\Delta(\vec{x},0),\varepsilon)$ that we know are

$$\begin{aligned} \langle f(\Delta(\vec{x},0),\varepsilon)\rangle &= 0 \\ \langle f(\Delta(\vec{x},0),\varepsilon)^2\rangle &= c_{\max}^2 \end{aligned} \tag{6.4}$$

In which < > denotes spatial averaging, c_{max} the maximum achievable speckle contrast.

Starting with the relation derived in [112](chapter 5) between the tagged fraction R_{diff} and the differences between the speckle patterns, we can write:

$$
\begin{aligned}
R_{diff} &\approx \tfrac{1}{8}\left\langle \left(I(\vec{x},0) - I(\vec{x},\pi/\omega) \right)^2 \right\rangle \\
&= \tfrac{1}{8}\left\langle \left(\Delta(\vec{x},0) - f\left(\Delta(\vec{x},0),\varepsilon\right) \right)^2 \right\rangle \\
&\quad \tfrac{1}{4}\left(c_{\max}^2 - \left\langle \Delta(\vec{x},0) f\left(\Delta(\vec{x},0),\varepsilon\right) \right\rangle \right)
\end{aligned}
\tag{6.5}
$$

To make this number independent of the speckle contrast we normalize with $c_{\max}^2$.

$$
\begin{aligned}
R_{diff,Norm} &= \frac{\left\langle \left(I(\vec{x},0) - I(\vec{x},\pi/\omega) \right)^2 \right\rangle}{8c_{\max}^2} \\
&= \tfrac{1}{4} - \frac{\left\langle \Delta(\vec{x},0) f\left(\Delta(\vec{x},0),\varepsilon\right) \right\rangle}{4c_{\max}^2}
\end{aligned}
\tag{6.6}
$$

The tagged fraction R_{sum} derived from the normalized speckle contrast from a two speckle pattern summation is given by [109]:

$$
\begin{aligned}
R_{sum} &\approx 1-\frac{\sqrt{\frac{\left\langle \left(I(\vec{x},0)+I(\vec{x},\pi/\omega)\right)^2\right\rangle}{\left\langle I(\vec{x},0)+I(\vec{x},\pi/\omega)\right\rangle^2}-1}}{c_{\max}} \\
&= 1-\frac{\sqrt{\frac{\left\langle \left(2+\Delta(\vec{x},0)+f(\Delta(\vec{x},0),\varepsilon)\right)^2\right\rangle}{4}-1}}{c_{\max}} \\
&= 1-\frac{\sqrt{\frac{4+\left\langle \Delta(\vec{x},0)^2\right\rangle+\left\langle f(\Delta(\vec{x},0),\varepsilon)^2\right\rangle+2\left\langle \Delta(\vec{x},0)f(\Delta(\vec{x},0),\varepsilon)\right\rangle}{4}-1}}{c_{\max}} \\
&= 1-\frac{\sqrt{\frac{1}{2}c_{\max}^2+\frac{1}{2}\left\langle \Delta(\vec{x},0)f(\Delta(\vec{x},0),\varepsilon)\right\rangle}}{c_{\max}} \\
&\approx 1-\frac{c_{\max}+\frac{\left\langle \Delta(\vec{x},0)f(\Delta(\vec{x},0),\varepsilon)\right\rangle}{4c_{\max}}-\frac{c_{\max}}{4}}{c_{\max}} \\
&= \frac{1}{4}-\frac{\left\langle \Delta(\vec{x},0)f(\Delta(\vec{x},0),\varepsilon)\right\rangle}{4c_{\max}^2}
\end{aligned}
\tag{6.7}
$$

The identity of equation 6.6 and equation 6.7 shows that the sum and subtraction methods give the same tagged fraction. However both methods are based on different terms of equation 6.1 that clearly contain the same information.

6.2.2 Correcting the estimations for non-ideal speckle patterns

Non-ideal and ideal speckle patterns differ in various ways. First, when we add a DC offset to the speckle pattern the speckle contrast is reduced. Next, the spatial sampling of the speckle pattern also influences the observed speckle contrast. The speckle contrast approaches unity when taking the limit of the number of pixels per speckle toward infinity[114]. The finite size of a camera pixel also reduces the speckle contrast because the measured intensity by the pixel is spatially averaged [115]. To overcome these problems in laser speckle contrast methods for perfusion imaging (LSCI) it is common to normalize the speckle contrast with the maximum achievable speckle contrast for the given setup. It was shown

that this approach works in LSCI[115] and in this study we show that it also works in acousto-optics, and that this procedure gives the correct estimation for the tagged fraction defined in Resink et al. [112].

$I_{t,ideal}$ is a speckle pattern that has a contrast for small tagged fractions R given by a model as: $c_{\mathrm{t,ideal}} \approx 1 - R$ [112]. From here on we omit the use of spatial coordinate $\vec{x}$ in the equations for readability.

We write the observed nonideal speckle pattern $I_{measured}$ as the sum of an ideal tagged speckle pattern $I_{t,ideal}$ and a speckle contrast distorting function γ, giving

$$I_{measured} = I_{t,\mathrm{ideal}} + \gamma \tag{6.8}$$

The resulting speckle contrast is thus for a normalized speckle pattern

$$\begin{aligned} c^2_{measured} &= \left\langle I^2_{measured} \right\rangle - 1 \\ &= \left\langle \left(I_{t,ideal} + \gamma \right)^2 \right\rangle - 1 \end{aligned} \tag{6.9}$$

This measured speckle pattern is corrected by normalizing it with the maximum contrast:

$$\begin{aligned} c^2_{corrected} &= \frac{c^2_{measured}}{c^2_{\max}} \\ &= \frac{\left\langle \left(I_{t,ideal} + \gamma \right)^2 \right\rangle - 1}{\left\langle \left(I_{u,ideal} + \gamma \right)^2 \right\rangle - 1} \\ &= \frac{\left\langle I^2_{t,ideal} \right\rangle + \left\langle \gamma^2 \right\rangle + 2\left\langle I_{t,ideal}\gamma \right\rangle - 1}{\left\langle I^2_{u,ideal} \right\rangle + \left\langle \gamma^2 \right\rangle + 2\left\langle I_{u,ideal}\gamma \right\rangle - 1} \end{aligned} \tag{6.10}$$

where $I_{u,ideal} = I_{t,ideal}$ if the tagged fraction is zero. When the average value of both $I_{t,ideal}$ and $I_{u,ideal}$ is the same, thus $\left\langle I_{\mathrm{t,ideal}} \right\rangle = \left\langle I_{u,\mathrm{ideal}} \right\rangle$ then the relation between $c_{t,ideal}$ and the two speckle patterns is given as:

$$\left\langle I_{t,ideal}^2 \right\rangle = \left\langle I_{u,ideal} \right\rangle^2 \left(c_{t,ideal}^2 + 1 \right)$$
$$\left\langle I_{u,ideal}^2 \right\rangle = 2\left\langle I_{u,ideal} \right\rangle^2 \tag{6.11}$$

By substituting this in equation 6.10 we obtain

$$c_{corrected}^2 = \frac{\left\langle I_{u,ideal} \right\rangle^2 \left(c_{t,ideal}^2 + 1 \right) + \left\langle \gamma^2 \right\rangle + 2\left\langle I_{t,ideal}\gamma \right\rangle - 1}{2\left\langle I_{u,ideal} \right\rangle^2 + \left\langle \gamma^2 \right\rangle + 2\left\langle I_{u,ideal}\gamma \right\rangle - 1} \tag{6.12}$$

We are interested in speckle contrast differences Δc between modulated and non-modulated speckle patterns, which for small values can be related to $\underline{c}$ as

$$\begin{aligned} c^2 &= \left(1 - \Delta c\right)^2 \\ &= 1 - 2\Delta c + \Delta c^2 \\ &\approx 1 - 2\Delta c \end{aligned} \tag{6.13}$$

Substituting equation 6.13 in equation 6.12 gives

$$1 - 2\Delta c_{corrected} = \frac{\left\langle I_{u,ideal} \right\rangle^2 \left(2 - 2\Delta c_{t,ideal} \right) + \left\langle \gamma^2 \right\rangle + 2\left\langle I_{t,ideal}\gamma \right\rangle - 1}{2\left\langle I_{u,ideal} \right\rangle^2 + \left\langle \gamma^2 \right\rangle + 2\left\langle I_{u,ideal}\gamma \right\rangle - 1}$$

(6.14)

Because all speckle patterns in this study are normalized we can write the following relations

$$\begin{aligned} \left\langle I_{t,ideal} + \gamma \right\rangle^2 &= 1 = \left\langle I_{t,ideal} \right\rangle^2 + \left\langle \gamma \right\rangle^2 + 2\left\langle I_{t,ideal}\gamma \right\rangle \\ \left\langle I_{u,ideal} + \gamma \right\rangle^2 &= 1 = \left\langle I_{u,ideal} \right\rangle^2 + \left\langle \gamma \right\rangle^2 + 2\left\langle I_{u,ideal}\gamma \right\rangle \end{aligned} \tag{6.15}$$

Because $\left\langle I_{\mathrm{t,ideal}} \right\rangle^2 = \left\langle I_{u,\mathrm{ideal}} \right\rangle^2$ we obtain

$$2\left\langle I_{t,ideal}\gamma \right\rangle = 2\left\langle I_{u,ideal}\gamma \right\rangle = 1 - \left\langle I_{u,ideal} \right\rangle^2 - \left\langle \gamma \right\rangle^2 \tag{6.16}$$

Therefore, we can simplify equation 14 by substituting this relation to obtain

$$\Delta c_{corrected}\left(1+\frac{\left\langle \gamma^2 \right\rangle - \left\langle \gamma \right\rangle^2}{\left\langle I_{u,ideal} \right\rangle^2}\right) = \Delta c_{t,ideal} \qquad (6.17)$$

Thus when the standard deviation of γ is small compared with the intensity of the ideal speckle pattern, the Δc after correction and the one predicted by the model are the same. This is the case for small errors induced by the finite size of pixels and for DC offsets. The measured contrast becomes higher when γ represents noise on the camera. When the SNR of the measured speckle pattern is high the standard deviation of γ is small compared to the average speckle intensity.

When we substitute a speckle pattern for γ that represents a second polarization, and γ thus depends on the tagged fraction like $I_{t,ideal}$ we have to derive this equation again in a similar way but we can now make the additional substitution $\left\langle \gamma^2 \right\rangle = \left\langle \gamma \right\rangle^2 \left(c_{t,ideal}^2 + 1\right)$ in equation 6.10. This substitution results in

$$\Delta c_{corrected} \approx \Delta c_{t,ideal} \qquad (6.18)$$

Both equations 6.17 and 6.18 show that $\Delta c_{t,ideal}$ and $\Delta c_{corrected}$ are very similar and thus that correction by normalizing over the maximum obtainable speckle contrast not only makes the measurement independent of the speckle contrast but also gives numerical values that satisfy the behavior of an ideal modulated speckle pattern as defined in [112]. Thus the first line of equation 6 and the first line of equation 6.7 give us the tagged fraction independent of the maximum speckle contrast for the subtraction and summation method. The maximum speckle contrast of the setup can be determined performing a measurement without ultrasound or on a static turbid sample.

6.3 Materials and methods

The similarity of equation 6.17 and 6.18 is tested experimentally. Therefore we use the setup and experimental results of [106], see figure 6.1. Briefly, the experimental setup consists of an injection seeded frequency doubled Nd:YAG laser with a pulse repetition rate of 10 Hz, wavelength of 532 nm and a Fourier limited pulse of 5 ns and a coherence length of approximately 1.5 m. We inject 5 cycles of 5 MHz ultrasound.

Speckle patterns were recorded with a camera that was placed behind the sample. Because of the repetition rate of the laser we sample 2 speckle patterns with 100 ms time separation. By timing the injection of ultrasound with the laser we make sure that the sound burst was at the optical plane when the laser fires and has either a 0 or π phase shift. An agar-intralipid phantom with $\mu_s' = 0.6\ mm^{-1}$ was used. This phantom is a 20 mm diameter cylinder making the 3 mm diameter optodes 20 mm apart.

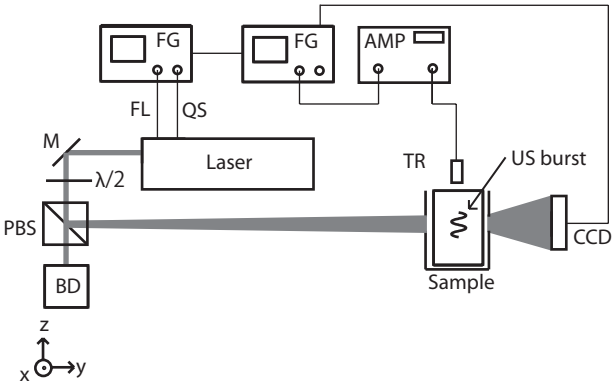

Figure 6.1. Experimental set-up. FG: function generators, AMP: amplifier, TR: Ultrasound transducer and BD: beam dump.

The relation between the summation and the subtraction method is then verified from the experimentally obtained speckle patterns. The data used for the verification was presented in [106] without the correction for the subtraction method. We performed a spatial scan in the plane perpendicular to the US propagation vector and between the optodes with a step size of 0.5 mm.

We also performed numerical simulations to show the validity of equations 6.17 and 6.18. For this purpose we constructed several modulated speckle patterns. The contrast of a speckle pattern that is influenced by a DC offset, finite pixel size or extra polarizations was investigated. We used a 300x300 pixel reference speckle pattern where the speckles are 3 pixels in size. These patterns are the result of 2500 interfering phasors that originate from random points within an aperture having a random and modulated phase. This approach is similar to the one we used in[112].

We numerically simulated two combined cases: one extreme and one with more realistic values. All these simulations where repeated 15 times

so that the standard deviation can be plotted as error bar. We set a tagged fraction R = 0.01 where all the phasors had the same phase modulation amplitude. The values obtained were corrected by normalizing by c_{max} for the summation and speckle contrast method (first step in equation 6.7) and c_{max}^2 for the subtraction method (equation 6.6). Several distortions can act on a speckle pattern to lower the speckle contrast, the case without any distortions was our reference. Therefore we tested our method for the summation of a DC value with a magnitude of 1,2, or 3 times the average intensity of the speckle pattern ('DC1', 'DC2' and 'DC3'). Further, a second polarization lowered the speckle contrast ('2 Pol'). The speckle size in terms of pixels per speckle (P/S) was 0.7 Pixels/Speckle ('0.7 P/S'), and 13 Pixels/Speckle ('13 P/S') compared with the 3 pixels per speckle of the reference. Further the finite size of pixels in a real camera lowers the contrast because of spatial averaging of small parts of the speckle pattern, this was simulated by convolving the speckle pattern with a square matrix of size N (N=3,5,7) where all elements where equal to 1. ('Blur 3', 'Blur 5', and 'Blur 7'). The simulation called 'All E' gave an extreme case of combined distortion, so 3 times the average value for the DC offset and 2 polarizations and 3 pixels per speckle and a blur matrix size of 7x7. And a more realistic case of combined distortions ('All R') was considered where the DC value was equal to the average speckle value (DC1) and 2 polarizations and a blur matrix size of 3.

6.4 Results

The maximum observed speckle contrast in this experiment was c_{max}=0.47. A plot of the median of 6 measurements per position of $R_{diff,Norm}$ (right) and R_{sum} (left) in figure 2 shows that the plots are nearly identical.

We plotted the pixel values against each other and found a near unity slope (figure 2 center plot).

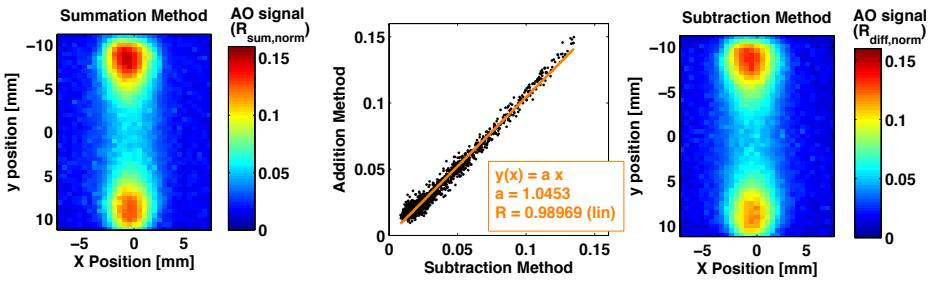

Figure 6.2. Estimated tagged fractions obtained with the summation method (left) and the subtraction method (right) compared against each other (center).

To illustrate the speckle patterns obtained from the simulation, in figure 3 we show the reference and realistic case as described above of 3 (sum, subtraction and contrast) speckle patterns, the first speckle pattern is obtained by adding two instantaneous speckle patterns at two opposite ultrasound phases, the second by subtraction of these phases, and the third is obtained by integration of the speckle field over a complete US cycle. The data comes from the simulated speckle pattern for the ideal case that is used as reference, the second set comes from the simulation for the more realistic case.

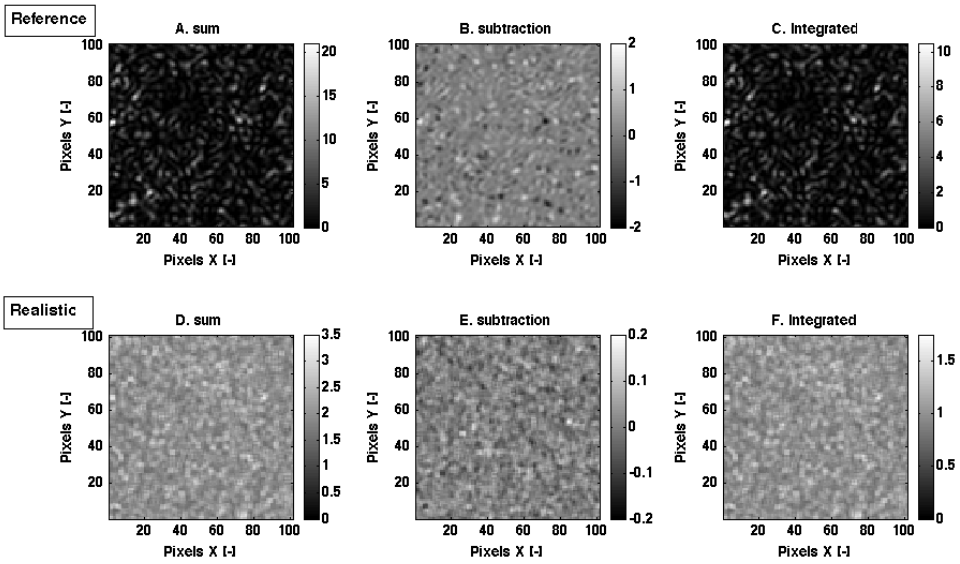

Figure 6.3. Two sets of cropped speckle patterns, the reference (top) and the realistic case (bottom), for the summated pattern (left), subtracted pattern (center) and integrated pattern that is used for the contrast method (right).

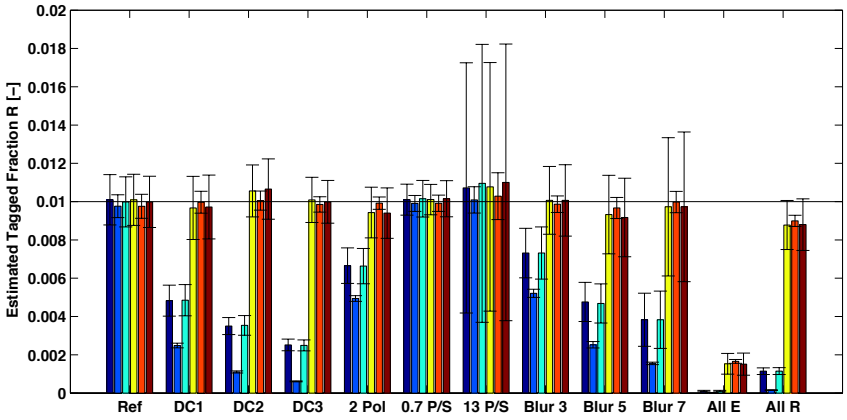

Figure 6.4. Estimated tagged fractions from simulated speckle patterns before and after correction, for the 3 methods for several contrast lowering mechanisms. Per mechanism 6 bars are given, from left to right: summation, subtraction, and speckle contrast method, followed by summation, subtraction, and speckle contrast method corrected with c_{max}.

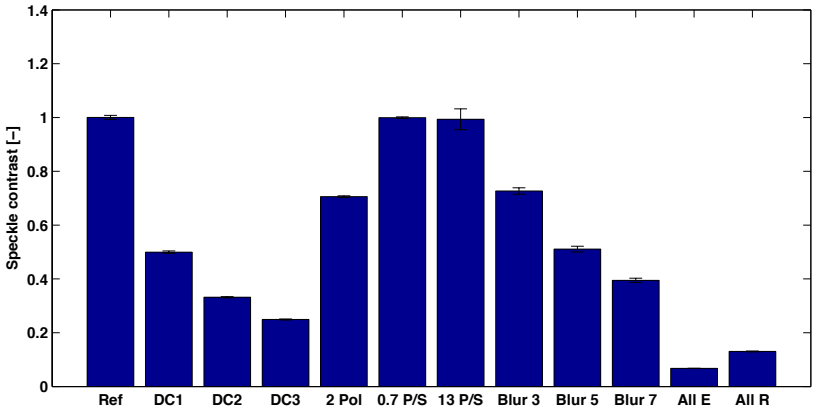

Figure 6.5. The speckle contrast values obtained from the simulations for the set of speckle contrast lowering mechanisms, working on the speckles without ultrasound modulation.

First of all we see in figure 6.4 that all of the values of the reference reproduce the set value of 0.01 for the tagged fraction. Figure 6.5 shows a speckle contrast of 1 for this reference. After correction the DC value has no influence on the estimated tagged fraction. The case of two polarizations is also predicting the correct value after correction. As shown in figure 6.5 the speckle contrast for this case is $\frac{1}{2}\sqrt{2}$ as expected. The

speckle contrast for the different speckle sizes is also unity because of the point sampling. The error bars in figure 6.4 are large in these cases because the amount of speckles on the camera decreases with the speckle size. The spatial averaging has a clear effect on the speckle contrast shown in figure 6.5 and causes a slight underestimation of the tagged fraction in figure 6.4. In the case of combined extreme distortions ('All E') the speckle contrast is very low and apparently the standard deviation of the contrast distorting function γ in equation 6.17 is too large to successfully recover the tagged fraction after correction. But the more realistic combined case ('All R'), for which the distortions consist of addition of a DC value equal that of the average intensity and blurring by convolution of 3x3 pixels and two polarizations, only gives a small underestimation of the tagged fraction.

6.5 Discussion and conclusion

We derived and validated a correction method to compensate AO measurements for reduced speckle contrast induced by non-ideal properties of the set-up. This compensation makes measurements comparable between different setups. By recording speckle patterns at two opposite phases of the ultrasound we are able to extract an AO signal by subtraction or addition of the two speckle patterns, see equation 6.6 and 6.7, in which the maximum obtainable speckle contrast c_{max} is used to correct The measured result for speckle contrast distortions. The maximum obtainable contrast c_{max} for a given setup must be determined experimentally. This can be done by performing a measurement without applying ultrasound on a very stable phantom.

We have shown (see figure 6.2) that tagged fractions obtained with the summation method and subtraction method in an experiment are in agreement with each other after applying our correction method. The slope between these methods was found to be 1.04 in figure 6.2 and is highly influenced by the accuracy of measurement of the maximum achievable speckle contrast estimation c_{max} that is used as normalization parameter.

The analytical expression of equation 6.17 shows that the reduction in speckle contrast after correction gives virtually the same value as predicted by the reference. This expression was tested with a set of simulations that show to which extent the type of speckle distortion and its magnitude influence the reliability of the correction. For a realistic case where the tagged fraction R was set to 0.01 the correction has shown to work and the set value of the tagged fraction R was restored with little deviation, see figure 6.4. We expect that this correction method is valid for a wide range of tagged fraction values and that we are limited by noise at the lower end of the range. And, at the higher end of the range we are limited by the distribution of phase modulation amplitudes over the aperture [112].

Because the AO values of a measurement with low contrast speckle patterns can be corrected to the values that we expect for ideal high contrast speckle patterns, we can determine the fraction of tagged light R in a speckle pattern. As a consequence we know the mean square of the phase modulation amplitude linking the measureable quantities to physical changes inside the medium. [112] This all makes our AO method better reproducible in case of different speckle contrast values between measurements and setups. In this way, quantifying acousto-optic signals becomes robust against influence DC offsets, finite pixels size differences, small camera readout noise and so on. When the influence is very large and a great degree of accuracy is required the standard deviation of the distortion pattern γ must be determined by simulation of speckle fields with a guessed γ such that it matches measured speckle statistics of static reference objects.

This work makes the acousto-optic part of our strategy of combining photoacoustics and acousto-optics more quantitative and shows that the two-pulse summation method is performing the same way as the speckle contrast method. The summation method and the subtraction method are compatible with pulsed lasers used for photoacoustic measurements. In figure 6.4, the estimation of tagged fraction R on simulated speckle patterns with the subtraction method shows less noise than the speckle contrast and summation method in figure 6.4 and may be the preferred strategy, although technically more challenging than the summation method since it requires that two speckle patterns of two laser pulses fired within the same US pulse are acquired separately in two separate camera frames.

7 Discussion and outlook

The use of short nanosecond pulses in this thesis was very different from the quasiCW light established in chapter 2. However, there are also similarities between our method and earlier established work. The speckle contrast method of [47] has similarities with our addition method presented in chapter 4 For both the contrast method and the addition method the intensity is integrated over a number of phases. In the contrast method a continuum of phases is used where we only used 2 discrete phases. Our difference method of chapter 3 shares the idea of capturing speckle patterns at different times from [24]. However, the analysis of the acquired speckle patterns is different and we don't need to integrate light over a long time on the camera to obtain these speckle patterns. Therefore we are potentially less sensitive to speckle decorrelation.

Chapter 3 showed the feasibility of using ns pulsed light to obtain AO signals. Here we used an injection seeded pulsed laser that provides us with coherent nanosecond laser pulses. These pulses have a sufficient coherence length and beam stability to ensure that the generated speckle patterns between shots are nearly identical. By acquiring speckle images for many axial positions of the ultrasound we effectively followed the ultrasound through the medium. The first experiment in section 3.4 showed that dark speckles contain relatively high higher harmonic signals compared with the brighter speckles. This effect might be important for AO applications that improve resolution by tuning in on higher harmonics [116] since these signals are not necessarily all coming from higher harmonic US. Further, other techniques that rely in dynamic speckle patterns might be sensitive for this effect and overestimate the frequency content of motion inside the medium. As with all pulsed lasers there are small pulse to pulse variations. The pulse energy variations are mostly compensated by normalising all the recorded speckle patterns. The beam pointing stability is influencing the signal the most. The larger the aperture at the sample the more critical this laser property becomes. Another point of consideration in selecting a laser system is the distribution of hotspots in the intensity profile; these should not vary too much between pulses.

The repetition rate of the injection seeded laser was too low to fire twice within the speckle correlation time of biological tissues. The delay line from chapter 4 solved this problem by splitting the laser pulse over two paths. One path was elongated by using mirrors before the two paths where recombined. In this case a delay time of 27 nanoseconds could be realized. Small errors in alignment between the pulses cause the two instantaneous speckle patterns at the camera to be slightly different. Additionally some lenses where used to compensate for the difference of wavefront curvature. The lenses and mirrors are not ideal and thus slightly reduce the quality of the pulses. This leads to an overestimation of the AO signal. Another improvement would be to increase the delay of the second pulse so that the second pulse arrives closer to π phase shift of the ultrasound. The use of a higher US frequency also makes sure that the second pulse arrives closer to π phase shift in the current setup but higher frequencies usually give lower AO signal. So, a more stable delay line that gives longer delay times and that ideally can be set within a range of a few nano-seconds to several hundreds of nano-seconds would be ideal.

In chapter 5 we derived the relation between phase modulation and the amount of tagged light. By our theory this tagged light is linked to the reduction of speckle contrast and increased difference between speckle patterns through the action of ultrasound modulation. The theory of chapter 5 was developed for speckle patterns that have a speckle contrast near unity. These relations where verified with simulations. Therefore we can now link the speckle observations to phase changes of the detected light. This can tell us more about the refractive index variation, and particle displacements. Because the model does not hold equally well at high tagging fractions for different phase modulation amplitude distributions it might be possible to say something about the distribution found in real experiments. By doubling the ultrasound intensity the tagged fraction should double as well. The increased mismatch between experiment and model will give a hint on the phase modulation amplitude distribution.

Chapter 6 builds further on these concepts and shows that the sum method and difference method give the same results after correction for non-unity speckle contrasts. This correction is necessary because the measured contrast usually differs from unity. The contrast reduction is caused by the finite size of the camera pixels, a small DC background, noise and the presence of a second polarization. It makes sense to record two speckle patterns and estimate the AO signal based on the sum and difference method. The outcome of both methods can be averaged, and is useful when it reduces the noise. Based on the simulations we see that the difference method has less noise than the contrast and sum methods. For low tagged fractions it makes sense to only use the outcome of the difference method. However, when a slow camera is used and it is not possible to obtain two separate speckle images for each of the tandem laser

pulses, the sum method is the best because this will be able to overcome the speckle decorrelation time. If the jitter on the camera trigger and the dead time is small enough it is advisable to record two images. This enables averaging of the sum method and difference method and the use of double the amount of photons that can be used, thus reducing shot noise before the camera frame is saturated.

This AO method can be implemented in combined AO-PA instruments to perform measurements on ex-vivo and in-vivo samples. For practical applications it is recommended to improve the stability of the delay line setup, or ideally find a laser system that can deliver two identical laser pulses within the speckle decorrelation time.

As with other AO methods [117] it must be possible after adding a reference arm to the setup to focus light back to the ultrasound focus. This increases the fluence at the US focus and thus both the AO and PA signals are expected to increase. This allows for improved sound light measurements. This extra fluence might also be used for other diagnoses and therapy. The high optical power of pulsed lasers might be especially useful for localized therapy by heating up unwanted tissues. With low power CW heating the heat diffusion would cause the target and surrounding tissues to heat up and get damaged.

Summary

Visible and near infrared light are useful in medical diagnosis applications because many molecular transition energies are associated with these optical frequencies. This light scatters in most biological tissues resulting in a poor resolution in imaging applications. Because ultrasound scatters orders of magnitude less than light its resolution is superior. By combining ultrasound and light it is possible to use the optical sensitivity with the superior resolution of ultrasound. One technique that combines both is photoacoustics, where light is absorbed and via the photoacoustic effect transformed into ultrasound. Images can be obtained by triangulating the sources of ultrasound with algorithms such as back projection and delay-and-sum. However, the photoacoustic signal strength depends on the local fluence at the absorbers position and the absorption coefficient. The background of this work is the requirement to compensate for fluence distributions and give a more objective image of optical absorption coefficient. To this end we combine photo acoustics with acousto-optics in a technique named Sound Light. With Sound Light we normalize the photo acoustic measurements with acousto-optic measurements, to correct for the local fluence.

In chapter 2 we give an overview of acousto-optic techniques. In general, coherent light is injected in the object under investigation. Ultrasound is injected as well and at the region of interest both light and sound interact causing optical phase modulation. These phase modulations are mainly caused by refractive index modulation and particle displacements causing the optical path length to be modulated. A part of the light that escapes the object is captured at an optical detector. Often a camera is used for its great number of detector elements, which enables averaging for noise reduction. The light that illuminates the camera forms a speckle pattern because the phase of the light was randomized by the many scattering events in the object. The speckle pattern is modulated because the phase of the light was modulated by the ultrasound. There are many methods to detect and quantify the magnitude of the speckle modulation and thus estimating the amount of so called tagged light. For example, some use holography based methods, digitally or with the addition of a photo refractive crystal. Others use cryogenically cooled crystals to create very narrow spectral filters.

A major obstacle for in-vivo use of acousto-optics is that a measurement must be performed within the so-called speckle decorrelation time. Most AO methods are not to meet this requirement, since biological tissue has a speckle decorrelation time below 1ms. The ones that are capable for in–vivo use have disadvantages that makes them less suitable

for our sound light application. They use lasers that are not compatible with photoacoustics and have typically long acquisition times because they follow a single speckle over time with a fast detector in order to calculate an autocorrelation function. This method has typically acquisition times between 0.5 and 5 seconds for a single measurement point as explained in section 4.4.

In chapter 3 we describe how we obtain an AO signal with the use of 2 short laser pulses from an injection seeded Nd:YAG laser which has a large coherence length. The timing of the second laser pulse was such that it interacts with the opposite phase of the ultrasound. We demonstrated the difference method in which we subtract two recorded speckle patterns and take the variance of this difference as a measure of tagged light. The second method that we presented was the addition method, in which we add the two speckle patterns and take the speckle contrast as a measure for the tagged light. Both methods show behavior similar with a CW speckle contrast method. In a very stable sample we were able to visualize the modulation of a speckle pattern while the ultrasound was propagating trough this sample. The results of that experiment also showed that the modulation of the speckle intensity depends on its local brightness. The lower the local intensity the higher the harmonic components in its signal were relative to the fundamental frequency component. For these experiments the two laser pulses were separated by 100 ms, which is too much for in-vivo use. However this chapter made clear the AO signals can be obtained with a laser suitable for generation of PA signals.

Chapter 4 shows a proof of concept of a setup capable of delivering two laser pulses with nearly identical phase fronts and intensity profiles within a single ultrasound cycle. We used a delay line to split the pulses from an injection seeded Nd:YAG laser over two paths, where one of these paths is 8 meters longer than the other. After combining the two paths we effectively created two pulses with 27 ns time separation. Because of the small time separation of the two pulses and the limitations of the used camera we were only able to use the addition method, capturing two speckle patterns in the same camera frame. The frequency of the ultrasound was only 5 MHz, thus the phase at the second laser pulse was much less than the optimal 180º phase shift. This resulted in a poor signal compared with the results from chapter 3. However we were able to perform acousto-optics in purely liquid scattering samples with a speckle decorrelation times even smaller than that of in-vivo cases.

In chapter 5 we derive the relation between the phase modulation induced by the ultrasound and the expected signal for the difference method and the speckle contrast method. We did this for speckle patterns that have a near unity contrast and are considered ideal. For phase modulations larger than 0.35 radians and thus higher amounts of tagged

light the relation doesn't hold. If this leads to an overestimation or underestimation of the phase modulation depends on the phase modulation distribution of the light escaping the medium. This distribution can change depending on the location of the ultrasound relative to the optodes.

For chapter 6 we investigated the relation (equations 6.6 and 6.7) between the addition and the difference method in case of non unity speckle contrast. Several aspects at the detection side of the setup can influence the speckle contrast such as the finite size of the camera pixels, the speckle size and the presence or absence of a polarizer. Simulations showed that both methods calculate, after correction for the 'low' speckle contrast, the same amount of tagged light and are correctly estimating the amount of phase modulation. Thus we have a reliable way of detecting tagged light in a quantitative way, and independent of experimental parameters such as speckle size.

Samenvatting

Zichtbaar en nabij-infrarood licht zijn nuttig voor de toepassing in medische diagnose omdat veel moleculaire overgangsenergieën worden geassocieerd met deze optische frequenties. Dit licht verstrooit in de meeste biologische weefsels wat resulteert in een slechte resolutie in beeldvormingstoepassingen. Omdat ultrageluid ordes van grootte minder verstrooit dan het licht is de resolutie superieur. Door ultrageluid en licht te combineren is het mogelijk de optische gevoeligheid en de superieure resolutie van ultrageluid gebruiken. Een techniek die beide combineert is foto-akoestiek, waar het licht wordt geabsorbeerd en dat via het foto-akoestische effect wordt omgezet in ultrageluid. Afbeeldingen kunnen worden verkregen door de plaats van de ultrageluidsbronnen te bepalen met driehoeksmetingen met algoritmen als terug projectie en vertraag-en-sommeer. De signaalsterkte is afhankelijk van de plaatselijke lichtsterkte op de locatie van de absorbers en de absorptiecoëfficiënt. De achtergrond van dit werk is het compenseren voor de verdeling kan de lichtsterkte en een meer objectief beeld van de optische absorptie-coëfficiënt geven. Daarom willen we foto-akoestiek combineren met akoestisch-optische metingen in een techniek genaamd Sound Light. Met Sound Light normaliseren we de foto-akoestische metingen met akoestisch-optische metingen om zo te corrigeren voor de lichtverdeling.

In hoofdstuk 2 geven we een overzicht van akoestisch-optische technieken. In het algemeen wordt het object dat wordt onderzocht beschenen met coherent licht. Ultrageluid wordt ook geïnjecteerd en op de plaats waar we in geïnteresseerd zijn is er interactie tussen zowel licht als geluid daardoor wordt het licht fasegemoduleerd. Deze fase modulaties worden vooral veroorzaakt door brekingsindex modulatie en deeltjes verplaatsingen, dit zorgt er voor dat de optische weglengte worden gemoduleerd. Een deel van het licht dat uit het object komt wordt gedetecteerd met een optische detector. Vaak wordt een camera gebruikt om zijn grote aantal detectie elementen zodat middeling voor ruisonderdrukking mogelijk wordt. Het licht dat de camera verlicht vormt een spikkelpatroon omdat de fase van het licht werd gerandomiseerd door de vele verstrooiingen in het object. Het spikkelpatroon wordt gemoduleerd, omdat de fase van het licht werd gemoduleerd door het ultrageluid. Er zijn vele methoden voor het detecteren en kwantificeren van de omvang van de spikkel modulatie en dus een schatting te maken het van zogenaamde gelabelde licht. Bijvoorbeeld, holografie gebaseerde methoden, digitaal of met toevoeging van een fotorefractief kristal. Anderen gebruiken cryogeen gekoeld kristallen om zeer smalle spectrale filters te maken.

Een belangrijk obstakel voor in vivo gebruik van akoestisch-optische metingen en derhalve voor sound light is dat een meting in de zogenaamde spikkel decorrelatie tijd moet worden uitgevoerd. De meeste AO methoden kunnen niet aan onze eis voor de spikkel decorrelatie snelheid voldoen omdat biologische weefsels spikkel decorrelatie snelheden hebben van enkele KHz. De methoden die tot in-vivo geschikt zijn hebben nadelen die ze minder geschikt maken voor onze sound light applicatie. Ze zijn niet compatibel met foto-akoestiek en hebben meestal lange meettijden.

In hoofdstuk 3 beschrijven we hoe we een AO signaal verkrijgen met het gebruik van 2 korte laserpulsen van een “injection seeded” Nd:YAG laser met een grote coherentie lengte. We deden dit door de timing van de tweede laserpuls zodanig te kiezen dat het interactie heeft met de tegenovergestelde fase van het ultrageluid. Wij toonden de verschil methode waarbij trekken we de opgenomen spikkel patronen van elkaar af en nemen we de variantie van dit verschil als maat voor het gelabelde licht. De tweede methode die we presenteerden was de optel methode, waarbij voegen we de twee spikkel patronen samen en nemen we het spikkel contrast als maat voor het gelabelde licht. Beide methoden vertonen vergelijkbaar gedrag met de CW spikkel contrast methode. In een zeer stabiel object waren wij in staat om de modulatie van een spikkelpatroon te visualiseren terwijl het ultageluid propageerde in dit object. De resultaten van dit experiment toonden ook aan dat de mate van modulatie van de spikkelintensiteit afhankelijk waren van de helderheid. Hoe donkerder de spikkel hoe hoger de harmonische componenten in het signaal ten opzichte van de fundamentele frequentie component. Voor deze experimenten werden de twee laserpulsen gescheiden door 100 ms, dat is te veel voor in vivo gebruik. Hoewel in dit hoofdstuk duidelijk werd dat AO signalen verkregen kunnen worden met een laser die geschikt is voor het genereren van PA signalen.

Hoofdstuk 4 toont een proof of concept van een opstelling dat twee laserpulsen kan leveren met bijna identieke fase fronten en intensiteit profielen binnen een enkele ultrageluid cyclus. We gebruikten een vertragingslijn om de pulsen van een “injection seeded” Nd:YAG laser te splitsen in twee paden, waarbij een van deze paden 8 meter langer is dan de andere. Na het combineren van de twee paden hebben we effectief twee pulsen gecreëerd met 27 ns tijd verschil. Vanwege het kleine tijdsinterval tussen de twee pulsen en de beperkingen van de gebruikte camera waren we alleen in staat om de optel methode te gebruiken door twee spikkel patronen in 1 camera beeld te vangen. De frequentie van het ultrageluid was slechts 5 MHz waardoor het fase verschil met het tweede laserpuls veel minder was dan de optimale 180° faseverschuiving. Dit resulteerde in een ruizig signaal vergeleken met de resultaten uit hoofdstuk 3. Maar we waren in staat om akoestisch-optische metingen uit te voeren in vloeibare

verstrooiende objecten met een spikkel decorrelatie tijd kleiner dan die van in-vivo gevallen.

In hoofdstuk 5 leiden we de relatie tussen de fasemodulatie dat geïnduceerd wordt door het ultrageluid en het verwachte signaal voor het verschil methode en spikkel contrast methode. We deden dit voor spikkel patronen die een contrast hebben van ongeveer één dat als ideaal worden beschouwd. Voor grotere fase modulaties dan 0.35 radialen en dus hogere bijdragen van gelabeld licht houdt de relatie niet stand. of zich dit vertaalt naar een over- of onderschatting van de fasemodulatie is afhankelijk van de fasemodulatie verdeling van het licht uit het medium. Deze verdeling kan veranderen afhankelijk van de locatie van het ultrageluid opzichte van de optoden.

Voor hoofdstuk 6 onderzochten we de relatie (vergelijking 6.6 en 6.7) tussen de optel en het verschil methode voor een niet ideaal spikkel contrast. Verscheidene aspecten aan de detectie zijde van de instelling kunnen de spikkel contrast beïnvloeden zoals de eindige grootte van de camera pixels, de spikkel omvang en aan- of afwezigheid van een polarisator. Simulaties laten zien dat beide methoden tonen na correctie voor de 'lage' spikkel contrast dezelfde hoeveelheid gelabelde licht en een konden een correcte schatting maken van fase modulatie. Zo hebben we een betrouwbare manier voor het meten gelabeld licht en onafhankelijk van experimentele parameters als de spikkel grootte.

Acknowledgements

This thesis was not possible without the help and support of many people. First of all I like to thank all current and former members of BMPI that contributed to my pleasant times there and fruitful discussions. On this page I like to express my gratitude more specific.

First of all my office mates, Michelle, Danielle and Wenfeng, thank you all for the nice conversations about all kinds of thinks and the lets get tea together times. Michelle, special thanks for planning journeys before I did, so I could copy most without much effort.

Of course I like to thank our technical staff for the help in the lab. And for providing an organised and safe working environment. Especially thanks to Erwin for the discussions, fun and help during these years. I still remember the time you had to bug fix our lab view program form home right before we would go to Amsterdam for some experiments.

A special thanks to Berkan, who's questions about speckle modulation gave rice to the speckle movie used for chapter 3. And the conversations about every thing in general and bikes in special.

Also thanks to our scientific staff, Wiendelt, Ton, Srirang and Ivo thanks for the discussions and questions during, and outside the work meeting. A large part of the input during those meetings where yours. A special thanks to Wiendelt for reading and correcting the countless iterations of my chapters and publications and the fast response times to e-mails.

Finally also thanks to my friends, family and in special Jane for believing in me, supporting me and waiting with dinner because of me.

I also like to acknowledge FOM for funding this project, and providing some useful courses during the years.

BMPI, all the best with your future research, hopefully my contribution proves to be useful in or outside the clinic at some point in the future and help many.

References

[1] L. H. V. Wang, Dis Markers **19**, 123 (2003).

[2] K. Maslov and L. V. Wang, J Biomed Opt **13**, 024006 (2008).

[3] M. Heijblom, J. M. Klaase, F. M. van den Engh, T. G. van Leeuwen, W. Steenbergen, and S. Manohar, Technol Cancer Res T **10**, 607 (2011).

[4] M. Heijblom et al., Proc Spie **8087** (2011).

[5] H. Ammari, E. Bossy, V. Jugnon, and H. Kang, Siam J Appl Math **71**, 676 (2011).

[6] A. Q. Bauer, R. E. Nothdurft, T. N. Erpelding, L. H. V. Wang, and J. P. Culver, J Biomed Opt **16** (2011).

[7] K. Daoudi, A. Hussain, E. Hondebrink, and W. Steenbergen, Optics Express **20**, 14117 (2012).

[8] A. Hussain, K. Daoudi, E. Hondebrink, and W. Steenbergen, (Optical Society of America, 2012), p. BM2B.5.

[9] F. A. Duck, *Physical properties of tissue* (Academic Press, London, 1990).

[10] C. G. A. Hoelen and F. F. M. de Mul, The Journal of the Acoustical Society of America **106**, 695 (1999).

[11] H. F. Zhang, K. Maslov, G. Stoica, and L. H. V. Wang, Nature Biotechnology **24**, 848 (2006).

[12] S. Manohar, A. Kharine, J. C. G. van Hespen, W. Steenbergen, and T. G. van Leeuwen, Phys Med Biol **50**, 2543 (2005).

[13] F. A. Marks, H. W. Tomlinson, and G. W. Brooksby, in *proc. SPIE*, edited by B. Chance, and R. R. Alfano (SPIE, Los Angeles, CA, USA, 1993), pp. 500.

[14] W. Leutz and G. Maret, Physica B **204**, 14 (1995).

[15] L. H. Wang, S. L. Jacques, and X. M. Zhao, Opt Lett **20**, 629 (1995).

[16] D. Dolfi and F.Micheron, International Patent WO 1989/000278 (1989).

[17] D. S. Elson, R. Li, C. Dunsby, R. Eckersley, and M. X. Tang, Interface Focus **1**, 632 (2011).

[18] A. Lev and B. G. Sfez, Opt Lett **27**, 473 (2002).

[19] C. Kim, K. H. Song, K. Maslov, and L. V. Wang, J Biomed Opt **14** (2009).

[20] A. Lev, Z. Kotler, and B. G. Sfez, Opt Lett **25**, 378 (2000).

[21] H. B. Fu, D. Xing, Y. G. Zeng, Y. Wang, and Q. Chen, Chinese Phys Lett **20**, 2165 (2003).

[22] E. Granot, A. Lev, Z. Kotler, B. G. Sfez, and H. Taitelbaum, J Opt Soc Am A **18**, 1962 (2001).

[23] G. Yao and L. H. V. Wang, Appl Optics **39**, 659 (2000).

[24] S. Leveque-Fort, Appl Optics **40**, 1029 (2001).

[25] F. Martelli, Light propagation through biological tissue and other diffusive media : theory, solutions, and software (SPIE Press, Bellingham, Wash., 2010).

[26] L. H. V. Wang, Opt Lett **26**, 1191 (2001).

[27] L. H. V. Wang, Phys Rev Lett **8704** (2001).

[28] S. Sakadzic and L. V. Wang, Phys Rev E **72** (2005).

[29] K. B. Krishnan, P. Fomitchov, S. J. Lomnes, M. Kollegal, and F. P. Jansen, edited by M. Analoui, and D. A. Dunn (SPIE, Boston, MA, USA, 2005), pp. 60090V.

[30] M. Kobayashi, T. Mizumoto, Y. Shibuya, M. Enomoto, and M. Takeda, Appl Phys Lett **89** (2006).

[31] G. D. Mahan, W. E. Engler, J. J. Tiemann, and E. Uzgiris, P Natl Acad Sci USA **95**, 14015 (1998).

[32] S. Sakadzic and L. H. V. Wang, Phys Rev E **66** (2002).

[33] R. Zemp, S. Sakadzic, and L. V. Wang, Phys Rev E **73** (2006).

[34] M. Allmaras and W. Bangerth, arXiv [math.AP] (2010).

[35] S. Sakadzic and L. H. V. Wang, Phys Rev E **74** (2006).

[36] S. Sakadzic and L. H. V. Wang, Phys Rev Lett **96** (2006).

[37] L. V. Wang and S. Sakadzic, J Opt Soc Am A **24**, 2797 (2007).

[38] J. Laufer, C. Elwell, D. Delpy, and P. Beard, Phys Med Biol **50**, 4409 (2005).

[39] A. Bratchenia, R. Molenaar, and R. P. H. Kooyman, Appl Phys Lett **92** (2008).

[40] M. S. Singh, P. K. Yalavarthy, R. M. Vasu, and K. Rajan, Med Phys **37**, 3744 (2010).

[41] J. M. Elazar and O. Steshenko, Opt Lett **33**, 131 (2008).

[42] C. H. Kim and L. V. Wang, Opt Lett **32**, 2285 (2007).

[43] T. S. Leung and S. Powell, J Biomed Opt **15**, 055007 (2010).

[44] S. Leveque, A. C. Boccara, M. Lebec, and H. Saint-Jalmes, Opt Lett **24**, 181 (1999).

[45] J. Selb, S. Leveque-Fort, L. Pottier, and A. C. Boccara, Cr Acad Sci Iv-Phys **2**, 1213 (2001).

[46] J. Li and L. V. Wang, Appl Optics **41**, 2079 (2002).

[47] J. Li, G. Ku, and L. H. V. Wang, Appl Optics **41**, 6030 (2002).

[48] A. Bratchenia, R. Molenaar, T. G. van Leeuwen, and R. P. H. Kooyman, J Biomed Opt **14** (2009).

[49] S. R. Kothapalli, S. Sakadzic, C. Kim, and L. V. Wang, Opt Lett **32**, 2351 (2007).

[50] S. Sakadzic and L. H. V. Wang, Opt Lett **29**, 2770 (2004).

[51] G. Rousseau, A. Blouin, and J. P. Monchalin, Opt Lett **34**, 3445 (2009).

[52] M. Gross, P. Goy, and M. Al-Koussa, Opt Lett **28**, 2482 (2003).

[53] M. Gross, M. Lesaffre, F. Ramaz, P. Delaye, G. Roosen, and A. C. Boccara, Eur Phys J E **28**, 173 (2009).

[54] M. Atlan, B. C. Forget, F. Ramaz, A. C. Boccara, and M. Gross, Opt Lett **30**, 1360 (2005).

[55] K. Creath, Appl Optics **24**, 3053 (1985).

[56] F. J. Blonigen, A. Nieva, C. A. DiMarzio, S. Manneville, L. Sui, G. Maguluri, T. W. Murray, and R. A. Roy, Appl Optics **44**, 3735 (2005).

[57] T. W. Murray, L. Sui, G. Maguluri, R. A. Roy, A. Nieva, F. Blonigen, and C. A. DiMarzio, Opt Lett **29**, 2509 (2004).

[58] M. Tziraki, R. Jones, P. M. W. French, D. D. Nolte, and M. R. Melloch, Appl Phys Lett **75**, 1363 (1999).

[59] M. Gross, F. Ramaz, B. C. Forget, M. Atlan, C. Boccara, P. Delaye, and G. Roosen, Optics Express **13**, 7097 (2005).

[60] P. X. Lai, R. A. Roy, and T. W. Murray, Opt Lett **34**, 2850 (2009).

[61] F. Ramaz, B. C. Forget, M. Atlan, A. C. Boccara, M. Gross, P. Delaye, and G. Roosen, Optics Express **12**, 5469 (2004).

[62] G. Rousseau, A. Blouin, and J. P. Monchalin, Optics Express **16**, 12577 (2008).

[63] Y. Z. Li, H. L. Zhang, C. H. Kim, K. H. Wagner, P. Hemmer, and L. V. Wang, Appl Phys Lett **93** (2008).

[64] M. Lesaffre, S. Farahi, M. Gross, P. Delaye, A. C. Boccara, and F. Ramaz, Optics Express **17**, 18211 (2009).

[65] S. Farahi, G. Montemezzani, A. A. Grabar, J. P. Huignard, and F. Ramaz, Opt Lett **35**, 1798 (2010).

[66] E. Bossy, L. Sui, T. W. Murray, and R. A. Roy, Opt Lett **30**, 744 (2005).

[67] L. Sui, R. A. Roy, C. A. DiMarzio, and T. W. Murray, Appl Optics **44**, 4041 (2005).

[68] M. J. Chi, J. P. Huignard, and P. M. Petersen, J Opt Soc Am B **26**, 1578 (2009).

[69] Y. Z. Li, P. Hemmer, C. H. Kim, H. L. Zhang, and L. H. V. Wang, Optics Express **16**, 14862 (2008).

[70] L. H. V. Wang and G. Ku, Opt Lett **23**, 975 (1998).

[71] G. Yao, S. L. Jiao, and L. V. Wang, Opt Lett **25**, 734 (2000).

[72] M. Gross, M. Lesaffre, S. Farahi, A. C. Boccara, and F. Ramaz, J Opt Soc Am A **28**, 1436 (2011).

[73] E. B. A. la Guillaume, S. Farahi, E. Bossy, M. Gross, and F. Ramaz, Opt Lett **37**, 3216 (2012).

[74] A. Lev and B. G. Sfez, Opt Lett **28**, 1549 (2003).

[75] R. Li, L. P. Song, D. S. Elson, and M. X. Tang, Opt Lett **35**, 2633 (2010).

[76] C. C. Weng, Eur Phys J-Appl Phys **50** (2010).

[77] P. Kuchment and L. Kunyansky, Inverse Probl Imag **4**, 665 (2010).

[78] J. Li and L. H. V. Wang, Appl Phys Lett **84**, 1597 (2004).

[79] G. Bal and J. C. Schotland, Phys Rev Lett **104** (2010).

[80] A. Bratchenia, R. Molenaar, T. G. van Leeuwen, and R. P. H. Kooyman, Opt Lett **36**, 1539 (2011).

[81] A. Bratchenia, R. Molenaar, and R. Kooyman, Laser Physics, 1 (2011).

[82] S. Gunadi and T. S. Leung, J Biomed Opt **16**, 127005 (2011).

[83] B. H. Yuan, J. Gamelin, and Q. Zhu, J Appl Phys **104** (2008).

[84] D. J. Hall, U. Sunar, and S. Farshchi-Heydari, The Open Optics Journal **2**, 75 (2008).

[85] B. H. Yuan, J Biomed Opt **14** (2009).

[86] B. H. Yuan, Med Phys **36**, 3455 (2009).

[87] B. H. Yuan and Y. A. Liu, J Biomed Opt **15** (2010).

[88] B. H. Yuan, Y. Liu, P. M. Mehl, and J. Vignola, Appl Phys Lett **95** (2009).

[89] S. J. Kirkpatrick, R. K. Wang, D. D. Duncan, M. Kulesz-Martin, and K. Lee, Optics Express **14**, 9770 (2006).

[90] E. Bossy, A. R. Funke, K. Daoudi, A. C. Boccara, M. Tanter, and M. Fink, Appl Phys Lett **90** (2007).

[91] K. Daoudi, A. C. Boccara, and E. Bossy, Appl Phys Lett **94** (2009).

[92] R. Li, D. S. Elson, C. Dunsby, R. Eckersley, and M. X. Tang, Optics Express **19**, 7299 (2011).

[93] M. S. Singh, K. Rajan, and R. M. Vasu, J Appl Phys **109** (2011).

[94] X. Xu, H. Liu, and L. V. Wang, Nat Photon **advance online publication** (2011).

[95] J. W. Tay, P. X. Lai, Y. Suzuki, and L. V. Wang, Sci Rep-Uk **4** (2014).

[96] B. Judkewitz, Y. M. Wang, R. Horstmeyer, A. Mathy, and C. H. Yang, Nat Photonics **7**, 300 (2013).

[97] M. Hisaka and Y. Sasakura, Jpn J Appl Phys **48** (2009).

[98] S. R. Kothapalli and L. H. V. Wang, J Biomed Opt **14** (2009).

[99] S. R. Kothapalli and L. H. V. Wang, J Biomed Opt **13** (2008).

[100] P. X. Lai, J. R. McLaughlan, A. B. Draudt, T. W. Murray, R. O. Cleveland, and R. A. Roy, Ultrasound Med Biol **37**, 239 (2011).

[101] T. Murray, P. Lai, and R. Roy, Annals of Biomedical Engineering, 1 (2011).

[102] A. Lev, E. Rubanov, B. Sfez, S. Shany, and A. J. Foldes, Opt Lett **30**, 1692 (2005).

[103] A. Lev and B. Sfez, J Opt Soc Am A **20**, 2347 (2003).

[104] S. G. Resink, A. C. Boccara, and W. Steenbergen, J Biomed Opt **17** (2012).

[105] M. Lesaffre, F. Jean, F. Ramaz, A. C. Boccara, M. Gross, P. Delaye, and G. Roosen, Optics Express **15**, 1030 (2007).

[106] S. G. Resink, E. Hondebrink, and W. Steenbergen, Optics Express **22**, 3564 (2014).

[107] I. Freund, M. Rosenbluh, and S. Feng, Phys Rev Lett **61**, 2328 (1988).

[108] A. Bratchenia, *Towards quantitative acoustic-optic imaging* (university of Twente, Enschede The Netherlands, 2010).

[109] S. Resink, E. Hondebrink, and W. Steenbergen, Opt Lett **39**, 6486 (2014).

[110] D. D. Duncan, S. J. Kirkpatrick, and R. K. Wang, J. Opt. Soc. Am. A **25**, 9 (2008).

[111] A. Hussain, K. Daoudi, E. Hondebrink, and W. Steenbergen, J Biomed Opt **19**, 066002 (2014).

[112] S. G. Resink and W. Steenbergen, Phys Med Biol **60**, 4371 (2015).

[113] D. Briers, D. D. Duncan, E. Hirst, S. J. Kirkpatrick, M. Larsson, W. Steenbergen, T. Stromberg, and O. B. Thompson, J Biomed Opt **18**, 066018 (2013).

[114] J. C. Ramirez-San-Juan, E. Mendez-Aguilar, N. Salazar-Hermenegildo, A. Fuentes-Garcia, R. Ramos-Garcia, and B. Choi, Biomed Opt Express **4**, 1883 (2013).

[115] O. Thompson, M. Andrews, and E. Hirst, Biomed Opt Express **2**, 1021 (2011).

[116] H. Ruan, M. L. Mather, and S. P. Morgan, Opt Lett **37**, 1658 (2012).

[117] X. A. Xu, H. L. Liu, and L. V. Wang, Nat Photonics **5**, 154 (2011).

List of publications

Peer reviewed publications

- **S. Resink**, and W. Steenbergen, "**Tandem pulsed acousto-optics: an analytical framework of modulated high contrast speckle patterns."** Phys. Med. Biol. Vol. 60, pp. 4371(2015)

- **S. Resink**, E. Hondebrink and W. Steenbergen, "**Solving the speckle decorrelation challenge in acousto-optic sensing using tandem nanosecond pulses within the ultrasound period**", Optics Letters, Vol. 39, Issue 22, pp. 6486-6489 (2014)

- **S. Resink**, E. Hondebrink, and W. Steenbergen, "**Towards acousto-optic tissue imaging with nanosecond laser pulses**," Opt. Express 22, 3564-3571 (2014)

- **S.G. Resink,** A.C. Boccara and W. Steenbergen, "**State-of-the art of acousto-optic sensing and imaging of turbid media**", J. Biomed. Opt. 17(4), 040901 (Apr 06, 2012).

- **S. Resink**, J. Jose, R. Willemink, C. Slump, W. Steenbergen, T. van Leeuwen, and S. Manohar, "**Multiple passive element enriched photoacoustic computed tomography,**" Opt. Lett. 36, 2809-2811 (2011).

- J. Jose, R. Willemink, **S. Resink**, D. Piras, J. van Hespen, C. Slump, W. Steenbergen, T. van Leeuwen, and S. Manohar, "**Passive element enriched photoacoustic computed tomography (PER PACT) for simultaneous imaging of acoustic propagation properties and light absorption,**" Opt. Express 19, 2093-2104 (2011).

Conference proceedings

- **S.G. Resink**; E. Hondebrink and W. Steenbergen, ” **Acousto-optic signal generation with a nanosecond pulsed laser** ", Proc. SPIE 8943, Photons Plus Ultrasound: Imaging and Sensing 2014, 89434K (March 3, 2014)

- **S.G. Resink** and W. Steenbergen, "**Developing a stochastic model for acousto-optic tissue imaging**", Proc. SPIE 8223, Photons Plus Ultrasound: Imaging and Sensing 2012, 82232I (February 9, 2012)

- J. Jose, R. Willemink, **S. Resink**, D. Piras, J. Van Hespen, T. Van Leeuwen, and S. Manohar, "**Simultaneous Imaging of Speed-of-Sound, Acoustic Attenuation and Optical Absorption Using a Computed Tomography Photoacoustic Imager,**" in Biomedical Optics and 3-D Imaging, OSA Technical Digest (CD) (Optical Society of America, 2010), paper BSuD5.

- J. Jose, R. Willemink, **S. Resink,** T. Maalderink, J. C. G. van Hespen, et al. "**Ultrasound-transmission parameter imaging in a photoacoustic imager**", Proc. SPIE 7371, Novel Optical Instrumentation for Biomedical Applications IV, 73710S (July 09, 2009)